UNIVERSITY OF CALIFORNIA
RIVERSIDE

Understanding Interactions Between Organophosphates and Nucleic Acids

A Thesis submitted in partial satisfaction
of the requirements for the degree of

Master of Science

in

Bioengineering

by

Samson Or

August 2015

Thesis Committee:

Dr. Ian Wheeldon, Chairperson
Dr. Xin Ge
Dr. Dimitrios Morikis

The Thesis of Samson Or is approved:

_____

_____

_____

Committee Chairperson

University of California, Riverside

ACKNOWLEDGEMENTS

I would like to express my deepest and warmest wishes to those who have provided invaluable assistance in helping me complete this degree. I would like to first like to thank my parents who has always shown me love and support through all the peaks and troughs of life. Next, I would like to commemorate my research group. The head of the research group, Dr. Ian Wheeldon, has given support, encouragement, training, insight, and has proved invaluable to help me grow as a researcher. I would like to thank Yingning Gao who convinced me into joining the lab as well as for her continued friendship and contribution to my project. I would like to thank all my present and past lab members/office mates, Aaron Toop, Jyun-Liang (Aaron) Lin, Jie Zhu, Leidy Palomec, Ann-Kathrin Loebs, Pankaj Ramnani, Nuvia Saucedo, Andrew Flores, Victor Gomez, Stephanie Eatinger, Scott Hernandez, Rene Henderson, Cory Schwartz, Louis Lancaster, Jan Schlemmer, Aaron Stein, Megan Cook, Brandon Simmons-Rawls, Jordan Hall, and Peter Van for their assistance, friendship, camaraderie, and collaborations in the lab. A very special thanks to Ron Gorham from Dr. Morikis' lab whom taught, assisted and introduced me to the Nanotemper device.

Additionally, I want to recognize the University of California, Riverside for fostering a unique, diverse, open learning culture for all of its students. I would like to thank the Department of Bioengineering for their acceptance into the program. In addition, I would also like to thank the staff and faculty of both the Department of Bioengineering and Chemical and Environmental Engineering for their support. Furthermore, I would like to show my appreciation to Dr. Morikis and Dr. Ge for their mentorship, teaching and for allowing us access to their laboratory for sharing of equipment. I would like to thank my undergraduate research advisor, Dr. Duncan Liew for introducing me to lab work and who gave me the unique experience of working with stem cells. I would also like to thank Dr. Eulgem and Dr. Todd Fiacco for their support in my graduate education. Finally, I would like to thank all of the friends I have met outside of the lab over the past 7 years I have stayed at University of California, Riverside with whom I have the pleasure of meeting and sharing many great everlasting memories. This work was supported by the Defense Threat Reduction Agency (DTRA) and the Bourns College of Engineering at the University of California, Riverside.

DEDICATION

I dedicate this work to Susan and Hei Or whom have worked so hard to give me the tools needed to be successful. I love you mom and dad.

ABSTRACT OF THE THESIS

Understanding Interactions Between
Organophosphates and Nucleic Acids

by

Samson Or

Master of Science, Graduate Program in Bioengineering
University of California, Riverside, August 2015
Dr. Ian Wheeldon, Chairperson

The toxicity of organophosphates (OPs) are well described. They cause neuronal overstimulation which can lead to death. OPs have become tools of suicide and weapons of war due to their ease of access in areas throughout the globe. Thankfully, there are drugs that can inhibit the activity of OPs at their source as well as treating certain symptoms related to exposure. However, current drugs can only treat those whom have already been affected. They do not provide preventative treatment and cannot destroy existing stockpiles. The overabundance of OPs exists because of their ability as herbicides, fungicides and insecticides. Presently, usage of many organophosphates has been banned in many countries but they are still used in certain agricultural areas. This

project proposes a novel type of bioscavenger that molecularly sort OPs and their byproducts towards complete enzymatic detoxification. This research precedes the eventual goal of using DNA as a biomolecular scaffold for multienzyme structures by modulating OP binding to increase the efficacy of multistep enzymatic degradation. The studies presented here ascribe short sequences of DNA being able to bind organophosphates as well as the fact that binding is probably sequence dependent. Insight from these experiments will lead to a better understanding of the molecular landscape of substrate-DNA interactions.

Table of Contents

LIST OF TABLES

LIST OF FIGURES

LIST OF APPENDICES

CHAPTER 1: INTRODUCTION

1.1 MOTIVATION

Organophosphates (OP) are esters of phosphoric acids. They are utilized in agriculture and household commodities as herbicides and insecticides. Mass proliferation of OPs in the agricultural industry have led to increased probability of human exposure for both primary users and consumers such as farmers and households, respectively.[1] Direct exposure as well as accidental OP poisoning from farm run offs and small traces in food may lead to acute neurological problems as a result of inhibition of acetylcholinesterase, which is necessary in returning active neurons to their resting state.[2] Although cases of accidental exposure leading to death from OPs are rare, the danger of weaponized forms of organophosphates is a very real threat. Tabun, Sarin and Soman are G-type nerve agents that were developed and mass produced in the late 1930s.[3] Since then, there has been demand for an effective means of destroying deployed, stockpiled and post-exposure organophosphates and their byproducts. Current treatment of OP poisoning involves a combination of atropine, an anti-cholinergic drug, diazepam, an anticonvulsant, and oxime drug remediation, which functions by reactivating acetylcholinesterase.[4] In cases of acute poisoning, atropine

may become ineffective due to innate immunity or lack of definitive dosage requirements. Additionally, oximes are unable to reactivate acetylcholinesterase when a time dependent process called “aging” occurs. [5] Stockpile destruction is currently handled by incineration which has the problem of releasing toxic pollutants. Attachment of enzymes to cryogels, nylon, macroporous glasses, and fabric material are also proposed as solutions for OP destruction but they cannot handle the destruction of their toxic intermediates.[6] The development of a novel type of bioscavenger that directs substrates and their intermediates towards enzymatic detoxification is described here. This research precedes the eventual goal of using DNA as a biomolecular scaffold for multienzyme structures by modulating OP binding to increase the efficacy of multistep enzymatic degradation. The studies presented here ascribe short sequences of DNA being able to bind organophosphates as well as the fact that binding is probably sequence dependent. Insight from these experiments will lead to a better understanding of the molecular landscape of substrate-DNA interactions.

1.2 OVERVIEW OF ORGANOPHOSPHATES

The OP family of compounds encompass a diverse group of chemicals that have key effects on biological function. It was not until the early 20th

century, they were discovered to possess toxic properties.[7] Their pathophysiological effects were first described in the early 1900s in Germany and then revealed to the world in the post-World War II era. Until the 2000s, OPs were marketed for controlling insect populations after many of the organochlorine insecticides were banned. They are a central component in fungicides and herbicides, but play a more profound role as insecticides and chemical nerve agents. Insecticide forms of organophosphates fall under the categories of phosphotriesters, thiophosphotriesters or phosphorothiolesters.[1] Phosphotriesters contain a phosphorous center with three ester O-linked groups. Thiophosphotriesters possess a double bonded sulfur instead of a double bonded oxygen linked to the phosphate center. Phosphorothiolesters have one or more of the oxy-linked esters replaced by sulfo-linked esters. These different types of organophosphates can be seen in (Figure 1-1).

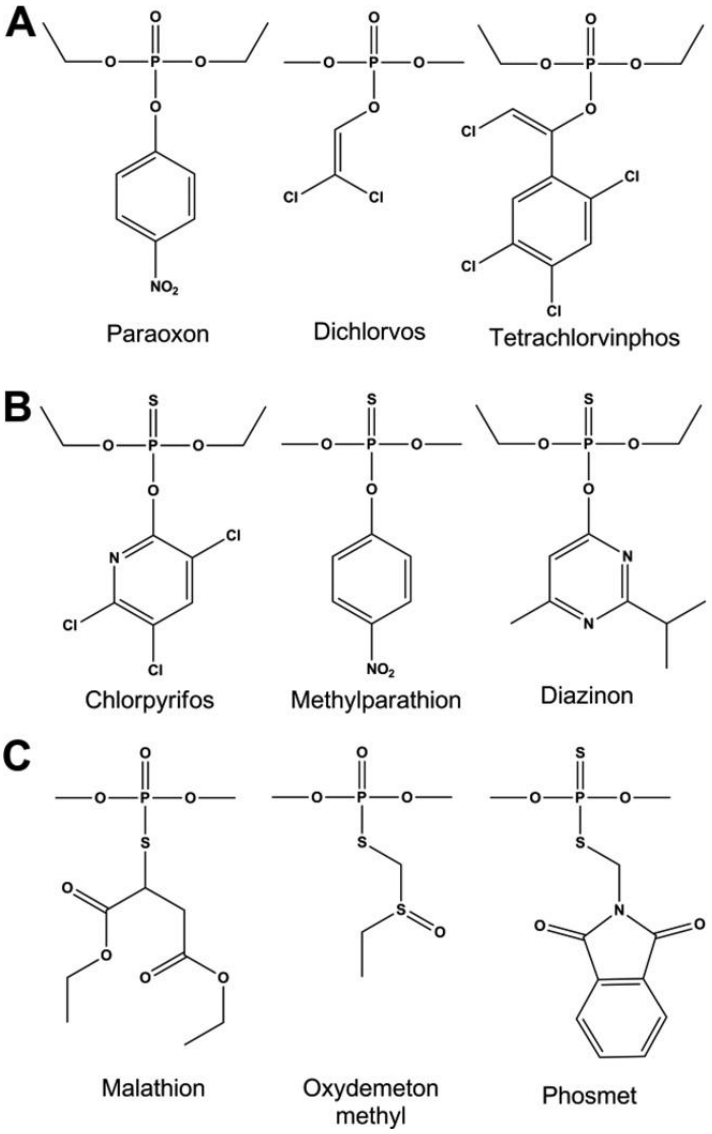

Figure 1-1: Structures of different organophosphates separated by category A) Phosphotriesters, B) Thiophosphotriesters, C) Phosphorothiolesters

The simple achiral structures that make up insecticides are in contrast to the OPs that are nerve agents (NAs). NAs exist as chiral phosphonate compounds without di-/tri- esters but instead a direct P-CH_3 linkage.[1]

Organophosphate toxicity arises primarily from inhibition of acetylcholinesterase, an enzyme which is vital for normal nerve function. Enzyme toxicity is attributed to the labile bond or leaving group present in the OP structure. The labile bond in the insecticides is usually the phenol or thiol group, which can be straight chained, branched or aromatic functional groups. Nerve agents on the other hand utilize fluoride or branched thiols as the leaving group in G type agents and V type agents respectively. Cleavage of the labile bond leads to irreversible inhibition in the active site of the enzyme acetylcholinesterase.[8] The positivity of the phosphoryl group plays an important role in determining their toxicity towards acetylcholinesterase as it is guided by the anionic site near the active site. The formation of a covalent P-O bond at a serine hydroxyl group in the active site impacts nerve terminals by causing an accumulation of acetylcholine, which can lead to seizures, paralysis, urination, salivation, and lacrimation. In serious cases of poisoning, it can cause respiratory failure leading to death. Figure 1-2 displays the cleavage of the labile bond and consequent blockage of the serine hydrolase on acetylcholinesterase.

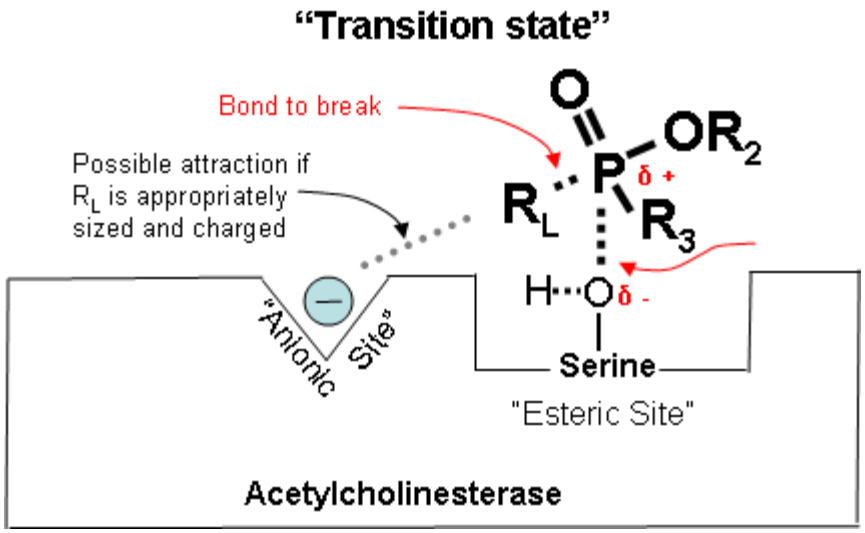

Figure 1-2: "Transition state" post organophosphate interaction with the active site serine on acetylcholinesterase

Current methods for treating OP poisoning includes the use of atropine, 2-PAM, and diazepam. Atropine is a competitor for the acetylcholine receptor.[9] Thus, when the atropine-receptor complex is formed, atropine antagonizes the excitatory effects of elevated acetylcholine due to loss acetylcholinesterase activity.[10] 2-PAM is an acetylcholinesterase reactivating oxime agent that functions through its nucleophilic activity. The nucleophile is able to attach to the anionic site near the esteric site where organophosphate inhibits acetylcholinesterase. If done promptly after OP exposure, 2-PAM can then bind to the organophosphate causing a conformational change which displaces it from the esteric site causing the enzyme to be functional again.

However, when the OP-attached enzyme is allowed to "age", a spontaneous loss of an alkyl group from the phosphorylated acetylcholinesterase occurs leading to an irreversibly inhibited enzyme.[11] The drug, diazepam, is used in conjunction with the former two drugs in cases of severe poisoning. It functions by preventing respiratory center overstimulation, as an anticonvulsant and it can also help ameliorate muscle fasciculation.[12] Ongoing efforts from medicinal chemists have focused on development of different types of pharmacological reactivators and sequestration against OPs. While these drugs can treat victims of OP poisoning post exposure, methods to decrease OP toxicity prophylactically and decontamination of existing stockpiles are equally important.

1.3 BIOCATALYST USAGE

As mentioned in the previous paragraph, there are several treatments for OP exposure. However, as a result of limited efficacy of pharmacological drugs *ex vivo*, their use in the destruction of stockpiled neurotoxins and function as prophylactic countermeasures is indeed complicated. Biocatalysts that intercept the OPs prior to their interaction with AchE would be preferable. Selection of an enzyme for the degradation of organophosphates is a challenging task since it must be able to act favorably under given conditions.

For example, one of the possible enzymes, butyrylcholinesterase (BChE) can degrade OPs, but it has high demands stoichiometrically, making it a less attractive option.[13] What this means is that one molecule of BChE is required to scavenge one molecule of organophosphate. Scientists have developed new strategies around the stoichiometric issues that BChE encountered by utilizing engineered enzymes like phosphotriesterases (PTE), phosphodiesterases (PDE), and organophosphate hydrolases (OPH) to selectively degrade toxic compounds.[14] [15] [16] Most hydrolases behave promiscuously leading to a low rate of hydrolysis for OPs. A good choice would be phosphotriesterase which originated in soil bacteria. Paraoxon is its natural substrate. Overuse of pesticides have triggered microorganisms to evolve enzymatic machinery to degrade OP compounds as a source of phosphorous.[17,18] Phosphotriesterase owes its broad substrate specificity to the design of its active site. The following describes the mechanism of PTE and the use of an engineered variant.

Phosphotriesterase from *Pseudomonas diminuta* is a zinc metalloenzyme that can effectively degrade a multitude of organophosphorous compounds. The enzyme was effectively crystallized and its x-ray structure appears to fold into a $(\beta/\alpha)_8$ barrel. PTE catalyzes the

destruction of OPs by function of a nucleophilic attack at the phosphorous center. There is a hydrolytic nucleophile activated as a hydroxide through ionization of a water molecule attached to α-metal ion. Amino acid residues Asp233, His254, and Asp301 are identified as the catalytic center. The metal ions present in the active site are able to increase the electrophilic character of the organophosphate by polarizing the double bonded oxygen or sulfur connected to the phosphate center. The stabilization of the Zn/Zn cation center is dependent on the pH with protonation leading to the collapse of bridging hydroxyl and loss of activity. The side chain positions of the amino acids present in the catalytic center are optimized to shuttle protons away from the active site.

The potential of PTE as a useful enzyme has substantiated over time, but one of the main problems it faces is the difficultly of expression. A mutated PTE denoted PTE-S5 is described here. PTE-S5 was discovered by Roodveldt and Tawfik. They found that the variant PTE-S5 possessing three point mutations resulted in a 20-fold higher functional expression than the native enzyme.[19] The main drawback of the variant is a decrease in thermal and metal coordinating stability, however, since the metal free PTE-S5 apo-enzyme is more stable, the ultimate yield of functional protein is higher. This

unique discovery undermines the wide assumption that the solubility of the fully processed protein is of great importance, in this case, it was the intermediate apo-protein which led to higher expression levels. When they were both overexpressed in the BL21 cells then lysed in zinc, PTE-S5 had higher activity than its WT counterpart as a result of the increased solubility of the apo-enzyme.[19] This variant, PTE-S5, would be chosen for experimental validation.

1.4 USE OF DNA AS A SCAFFOLD FOR MULTI ENZYME DEGRADATION

Living organisms utilize unique substrate-charge interactions and localization of proteins to facilitate and enhance complex processes essential to life. Two poignant examples are superoxide dismutase (SOD) and the bifunctional enzyme thymidylate synthase-dihydrofolate reductase (TS-DHFR).[20] SOD exploits substrate-enzyme interactions by using charge complementarity to enhance kinetics by directing superoxide into the small active site pocket of the enzyme. The enzyme TS-DHFR possesses two monomers, each containing two domains. It utilizes positive electrostatic potential of basic amino acid residues exposed to the solvent which restricts the diffusion of dihydrofolate, a negatively charged intermediate, through a

pre-defined channel between the two active sites.[21] Though researchers have made significant strides in the design of surface controlled diffusion pathways and chemical gradient generators, such schemes do not allow scaling down to the sub-10 nm range required for engineering synthetic enzyme pathways. An innovative approach to access the sub-10 nm scale is proposed here.

Depending on cell type and subcellular localization, cell surfaces are organized with localized proteins such as, hormone receptors, ion channels, and cell adhesion receptors that accomplish a wide variety of functions. Proteins anchored to a scaffold increase the likelihood of interaction that a cell has to the extracellular environment.[22] Thus, the spatial design of proteins against a membrane scaffold allows for increased probability of substrate availability and responding to the external environment.[23] The central hypothesis is that catalytic proteins or enzymes can be assembled in a manner that is analogous to natural membranes but instead with biomolecular DNA scaffolds. Prominent work in DNA nanotechnology have led to surface controlled diffusion paths and chemical gradient generators as strategies to control diffusion in the microscale.[24] [25] The availability of groove pockets, charged electrostatic interactions and areas of intercalation makes DNA a prime candidate. Groove pockets are present in the major and minor groove.

The major and minor groove is a byproduct of the non-symmetric helical structure of DNA. The predominant form of DNA is B-form which has a major groove length of approximately 22 Å and minor groove length of 12 Å. The former mentioned groove being commonly associated with protein-DNA interaction and the latter of which is related with small molecule binding.[26] The interaction could proceed in the groove via hydrogen bonding or van der Waals interactions. The negatively charged phosphate backbone can also play a role in small molecule binding by attracting positively charged moieties.[27] Intercalation is another method by which molecules can interact with DNA. This method of binding is characterized by conjugated, fused, planar ring systems that resemble the base pairs of DNA.

The application of enzyme-DNA nanostructures is a concept that has been previously built upon in our laboratory. The study included binding interactions between two substrates tetramethylbenzidine (TMB) and ABTS. It was found that TMB could bind to different DNA sequences while ABTS could not. When the DNA sequences were conjugated to horseradish peroxidase (HRP), this caused an increase in the rate leading to reduction in the apparent Michaelis constant.[28] The hypothesis is similar, by introducing beneficial interactions between an enzyme and its substrate, the effective

molarity of a substrate can be increased which leads to a corresponding decrease in the apparent binding constant as well as an increase in catalytic efficiency. By tuning the interaction with OPs using DNA scaffolds, the diffusion of toxins and their degradation products can lead to rapid, complete detoxification. This novel usage of DNA-enzyme molecular interactions should increase the local concentration of a particular substrate towards an enzyme that is tuned for degrading it. Our hypothesis will hopefully spearhead the development of a new generation of prophylactic countermeasures and stockpile detoxification.

1.5 OBJECTIVES

Organophosphates are a group of dangerous neurotoxic compounds. DNA molecular scaffolds arises as a potentially useful tool for binding OPs. The overall goal of this thesis is the development of a novel method of organophosphate degradation. Specifically, whether organophosphates bind to DNA remains to be seen. This work investigates the binding of OPs to DNA in addition to determining presence of sequence dependent binding.

Chapter 1, this chapter, provides an introduction to the motivation towards the desire of OP destruction. A brief overview of OPs as well as the

current methods for handling OP toxicity is discussed, as well as the shortcomings of current methods of OP detoxification. Possible enzymes that can be used for OP destruction are mentioned. Previously reviewed work in our lab as well as two examples of how nature handles substrate diffusion are discussed. This chapter also includes background information about DNA and its ability to bind small molecules. Lastly, the objective of the thesis for each chapter is presented.

Chapter 2 presents the study of fifty randomly generated different DNA sequences and three organophosphates and two byproducts of organophosphates are analyzed through a binding prediction software, AutoDock. Next, experimental validation using three chosen DNA sequences, DNA1, DNA2, DNA3 is determined by two other methods, microscale thermophoresis, fluorescence studies and circular dichroism.

Chapter 3 provides the experimental determination of the presence of sequence dependent binding of a single organophosphate, paraoxon. Several spectroscopic methods including Fourier transform-infrared spectroscopy, fluorescence studies, circular dichroism is performed. Circular dichroism this

time utilizes base repeats to determine preferential areas of binding rather than a randomly generated sequence.

Finally, the studies in chapters 1-3 are summarized and recommendations for future work are given in chapter 4.

CHAPTER 2: IDENTIFICATION AND VALIDATION OF DOUBLE STRANDED DNA THAT BIND ORGANOPHOSPHATES

2.1 INTRODUCTION TO AUTODOCK

Based on previous evidence in our lab which describes the binding between double stranded DNA to TMB and ABTS, we wanted to see if it was possible for organophosphates to bind to DNA.[28] For this project, three organophosphates and two byproducts were screened for DNA interaction. The goal was to predict organophosphate interactions to small 10 bp DNA sequences.

AutoDock is a suite of automated docking tools that includes both AutoDock and AutoDock Vina. AutoDock uses AutoGrid to search for possible binding locations while AutoDock Vina calculates grids internally, making it faster than AutoDock. Reasoning for the usage of one of the aforementioned programs over the other will be investigated. Autodock 4.2, uses the Lamarckian Genetic Algorithm (LGA) and the empirical free energy function to predict ligand, OP, docking to DNA. [29] The Lamarckian GA attempts to search for possible conformations while the empirical free energy function applies a semi-empirical force field to evaluate the binding by

estimating the intramolecular energy needed to transition from the unbound to the bound state and the intermolecular energetics of combining the OP and DNA in the bound state. AutoDock Vina inherits some of the same ideas and approaches of AutoDock, but different source codes, scoring functions, and actual algorithms differentiates the two. The results are graded and the coordinates for the best predicted binding energy in each cluster is noted. Independent of the program that will be selected for simulations, fifty randomly generated 10 bp sequences will be screened by pairing OPs and their byproducts to various sequences of DNA. The binding constants of OPs to small lengths of DNA varied which with in a sequence dependent manner was questioned.

The OPs that were investigated were paraoxon, methyl parathion, and fensulfothion. These three organophosphates share the feature of an ester linked aromatic labile carbon ringed structure with a characteristic planar shape connected a phosphate base center. As part of the overall objective of complete detoxification of OP compounds, the byproducts of paraoxon, *p*-nitrophenol and diethyl hydrogen phosphate were also surveyed for their DNA binding ability. The structures of three OPs that will be used as well as the toxic intermediates of paraoxon are shown in (Figure 2-1).

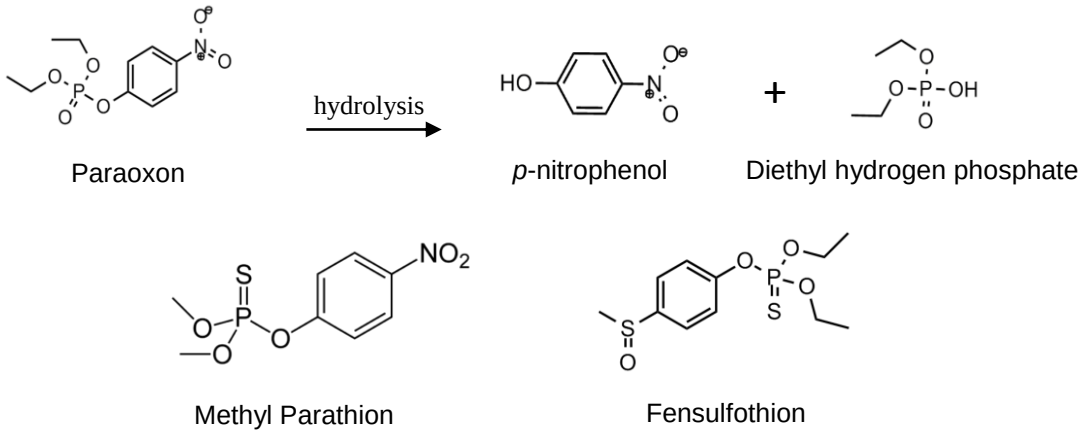

Figure 2-1: Structures of organophosphates and their hydrolysis products. Only the hydrolysis products of paraoxon will be examined.

2.2 METHODS OF EXPERIMENTAL DETERMINATION OF K_d's

After establishing the potential of organophosphate DNA binding, a method for experimentally determining binding constants *in vitro* was sought out. Current methods of finding binding affinity include isothermal titration calorimetry (ITC), surface plasmon resonance (SPR), fluorescence anisotropy (FA), and fluorescence correlation spectroscopy (FCS). Each of these methods have advantages and drawbacks, but access to these often specialized, expensive equipment was the major hurdle in their usage. Previous work in our laboratory demonstrated that DNA and small molecule interactions 4-NBH, NMN and TMB can be detected using UV-Vis titration. In an attempt to obtain the preliminary binding results, UV-Vis titration was employed for

predictions of binding constants for organophosphates and byproducts. Some substrates did not exhibit absorption in UV range and some possessed inherent overlapping wavelengths with DNA at around 260 nm which made determination of a binding constant impossible. The availability of the machine, Nanotemper Monolith NT.115 revitalized the project.

The Nanotemper uses Microscale Thermophoresis (MST) to determine binding constants based on charge, hydration shell and solvation entropy. MST is a highly sensitive method that allows detection of interactions in solution without the need for surface based immobilization. Microscale meaning it can be used to measure small particles and thermophoresis which is a phenomenon observed in all phases of matter when particles respond to changes in a temperature gradient. Specifically, in the case of small molecule-DNA interaction, the method involves measuring the changes in thermophoresis of DNA with increasing amounts of OP. The method has been used in multiple published articles involving fluorescently labeled protein and substrate interaction, but thus far have not been used frequently for studying DNA-small molecule interaction.[30] In the earlier case, the protein serves as the receptor and is fluorescently labeled for detection of thermophoresis. Fluorescently labeled DNA will be used as the receptor target with increasing

concentrations of organophosphate. This means that it is possible to figure out a broad sense where the binding of DNA is actually occurring and is non-specific to the defined areas of binding, either in the groove or intercalation. We additionally determined the binding constant of DNA and OP using a different method involving fluorescent probes aptly named "fluorescence studies".

Fluorescence studies utilize fluorescent probes to allow the study of interactions between macromolecules and small molecules. At this point, the identification of a probe that exhibits fluorescence is needed. The most prevalent fluorophore known to bind to DNA is Ethidium Bromide (EtBr), but its oncogenic effects combined with the toxicity of OPs and byproducts would be too dangerous to use in a university lab setting. Recently, methylene blue (MB) has replaced EtBr as the preferred probe due to it being a safer reagent.[31] Like EtBr, methylene blue binds to DNA through intercalation between the bases. By itself, methylene blue exhibits fluorescence, but when combined with DNA the fluorescence probe is quenched by DNA bases. This occurs because of the stabilization of the excited-electronic state electronic when freely diffusing MB and DNA interact to form the MB-DNA complex [32] When OPs or byproducts are added, assuming they bind in the same location as

methylene blue, the fluorophore will be displaced leading to increases in fluorescence. Further binding information can be obtained through circular dichroism (CD).

Circular dichroism is a powerful tool that exploits the chirality of DNA. Changes in absorption of right-handed and left-handed circularly polarized light allows for conformational monitoring. While the method is unable to determine structural information on molecules at an atomic level, it can be used in empirical studies with DNA.[33] The most frequently observed conformation of DNA is its B-form. Canonical B-form CD spectra has four characteristic bands around 210 nm, 220 nm, a negative band at 245 nm and a positive band at 275 nm. Organophosphates or their byproducts interacting with DNA may cause [hypo- or hyper-] chromic shifts, which are decreases or increases in peak intensity.[34]

2.3 METHODS

2.3.1 Chemicals

Paraoxon-Ethyl, Methyl Parathion, Fensulfothion, and Methylene Blue were purchased from Sigma-Aldrich (St. Louis, MO). P-nitrophenol was purchased from Acros Organics. Diethyl hydrogen phosphate was purchased

from Ark Pharm Inc. Oligonucleotides DNA1 $(CAGGTTGCAG)_2$, DNA2 $(GAATCTTCGG)_2$, DNA3 $(CCTAAAAGAG)_2$, cy5 labeled DNA1, DNA2 and DNA3 were purchased from Integrated DNA Technologies (IDT).

2.3.2 Experimental Set Up

Substrate-DNA Docking Simulations

Molecular docking simulations involving 10-bp and 20-bp oligonucleotides were used to examine the binding of substrates to DNA. Docking studies were carried out using AutoDock Vina and AutoDock 4.2 software. Compounds including organophosphates and its byproducts were downloaded from ChemSpider. The Lamarckian genetic algorithm (LGA) which was proven to be reliable and efficient was chosen for AutoDock 4.2 simulations. To compare AutoDock and AutoDock Vina, ten random 20-bp oligonucleotide sequences were generated for on the 3D-DART webserver to build 3d structural models.[35] To observe the binding between OPs and DNA, fifty random 10-bp oligonucleotide sequences were also generated. All water molecules were removed and Gasteiger charges and polar hydrogen atoms were added using AutoDockTools (ADT). AutoGrid was used to calculate affinity grids to the entirety of the grid map containing DNA-Substrate (60 x 60 x 100) with points of separation of 0.375 Å. Only the flexibility of the OPs

were taken into account and rotatable bonds without resonance were allowed to rotate. Each LGA job consisted of 30 or more runs, using an initial population of 150 individuals, 2.5 x 10^6 energy evaluations, 2.7 x 10^4 maximum number of iterations, 0.02 mutation rate, and 0.80 crossover rate. The molecular docking using default parameters was initiated. After each docking, all docking poses were clustered and arranged in groups where the poses with the lowest binding energy were arranged in tabular form. The dissociation constant was calculated using the Gibbs free energy equation using the free energy of binding.

Microscale Thermophoresis

Microscale thermophoresis (MST) measurements were done using the Monolith NT.115 instrument. Cy5-labeled single stranded DNA1, DNA2, DNA3 was duplexed to its complementary non-labeled strand. These were prepared by a denaturation and annealing step. Sixteen PCR tubes containing OPs or byproducts with each of the labeled DNA are prepared via serial dilution. Dilution of OPs and byproducts are specified by the K_d concentration finder from Nanotemper GmbH website based on their predicted dissociation constants from AutoDock. Sixteen standard treated Monolith capillaries were filled with corresponding PCR tube mix. Capillary

scans are taken to verify the normalized fluorescence and ensure no sample sticking. Buffer composition checks were made to ensure good reproducibility of MST results. MST optimized buffer is used which contains 50 mM Tris-HCl, 150 mM NaCl, 10 mM $MgCl_2$, 0.05 % Tween-20. In the case of Methyl Parathion, 98% MST buffer and 2% DMSO was used. Multiple runs using various MST powers were run and the best one is shown. Each data set contains a total of three repeats. Corresponding data to each run were analyzed using the Nanotemper Analysis software then exported to a text file.

Fluorescence Studies

Fluorescence studies were done using a BioTek Synergy 4 microplate reader. Each plate contained 96 to 384 well plates that hold a maximum of 100 µL per well. DNA1, DNA2, DNA3 were prepared by denaturation then a series of steps involving cooling. The probe that was used was methylene blue (10 µM). DNA1, DNA2, DNA3 (2.5 µM) was added to well containing methylene blue. This was followed by multiple wells with DNA and methylene blue where different concentrations of substrate were 2.5, 5, 7.5, 10, 25, 50, 100, 250 µM of OP or their byproducts were added. After thorough mixing through pipette, these solutions were inserted into the plate reader

where they were shaken for 8 seconds then allowed 8 minutes to equilibrate. The fluorescence emission spectra were then measured by using an excitation wavelength at 615 nm in the range of 645 to 745 nm. A blank containing buffer PB was subtracted to correct background fluorescence. Tabulated results were exported in an excel file where they would be further analyzed.

Circular Dichroism Spectroscopy

Circular dichroism (CD) measurements were made on a Jasco J-815 CD spectrometer. These were done under a constant stream of nitrogen to purge water vapor from the sample chamber. Continuous accumulation of CD spectra at wavelengths 500 nm to 190 nm was taken. DNA1, DNA2, DNA3 (40 μM) spectra without any OPs or byproducts were first measured. This was then followed by the addition of OPs and their byproducts up to 10 mM. The software used was provided by Jasco for instrument control and data acquisition. The scans were done at room temperature in phosphate buffer using a 1 cm quartz cuvettes. A spectrum of phosphate buffer solution was also recorded and subtracted from the spectra of DNA and DNA-substrate complexes. For each spectrum, 5-10 runs were averaged with a 5 minute equilibration time before each scan. Values for the CD spectra were exported in a comma separated value file for use in excel.

2.4 RESULTS & DISCUSSION

2.4.1 MOLECULAR DOCKING

Interactions between chemical species and DNA vary due to electrostatic and steric effects. Molecular simulations can predict the most probable binding sites and serve as an efficient tool for biophysical research. As mentioned earlier, AutoDock is a suite of docking tools that includes both AutoDock and AutoDock Vina. Since the scoring functions for the two programs are different, either program can give better results. In order to compare the two, binding results are obtained from AutoDock Vina and AutoDock. Docking examples examined ten different compounds binding to randomly generated 20-bp sequences. This is seen in (Figure 2-2).

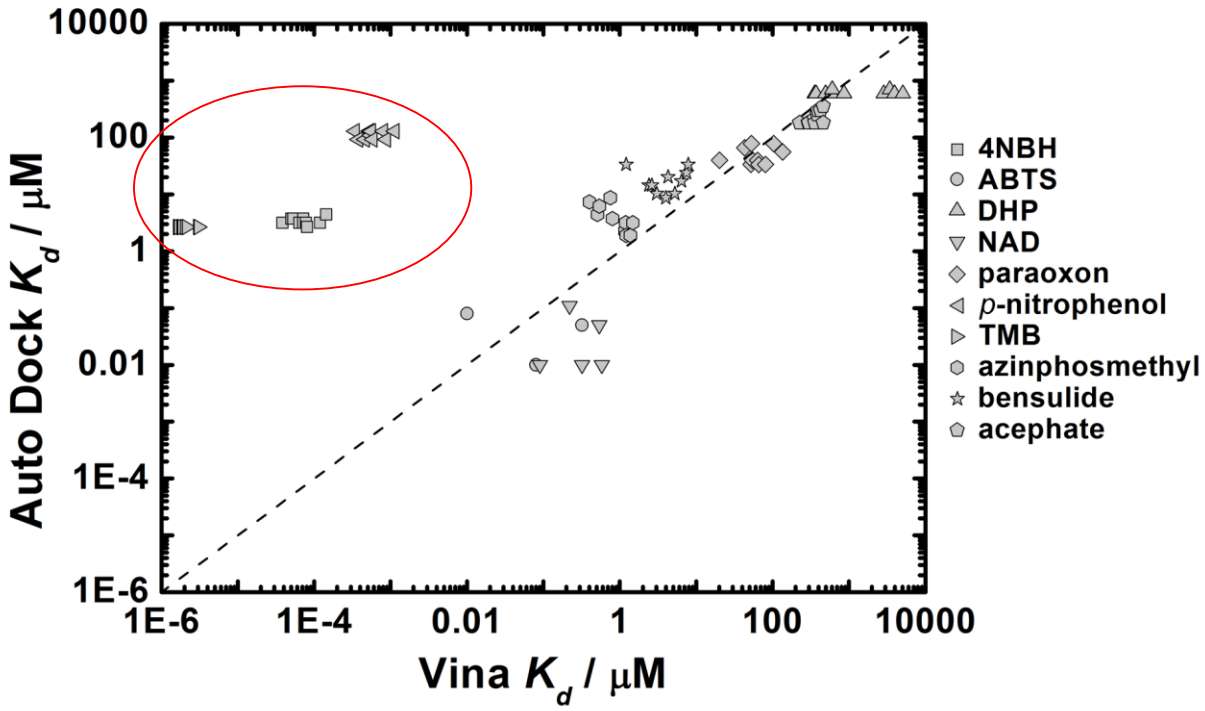

Figure 2-2: Comparison of binding constants obtained from AutoDock and AutoDock Vina

Binding energies were converted to dissociation constants for easy interpretation. A lower dissociation constant indicates tight binding, while a higher dissociation constant indicates weaker binding. Based on these results, it is possible to see that the majority of the predictions between AutoDock and AutoDock Vina are similar as indicated by the diagonal dotted line passing through the center. The values that were not similar are circled in red. Previous measurements done in our lab are in agreement with

the values obtained from AutoDock, thus we decided to proceed with AutoDock as the method of simulation.

In order to provide a theoretical support to the mode of binding for the toxins, AutoDock simulations were made according to the specifications mentioned earlier. Fifty randomly generated 10 bp sequences were chosen to examine the effects of different base pairs towards organophosphate binding. These results were tabulated and presented in (Figure 2-3). An example of one of the docked configurations of Paraoxon to one of the tested sequences is shown in (Figure 2-4).

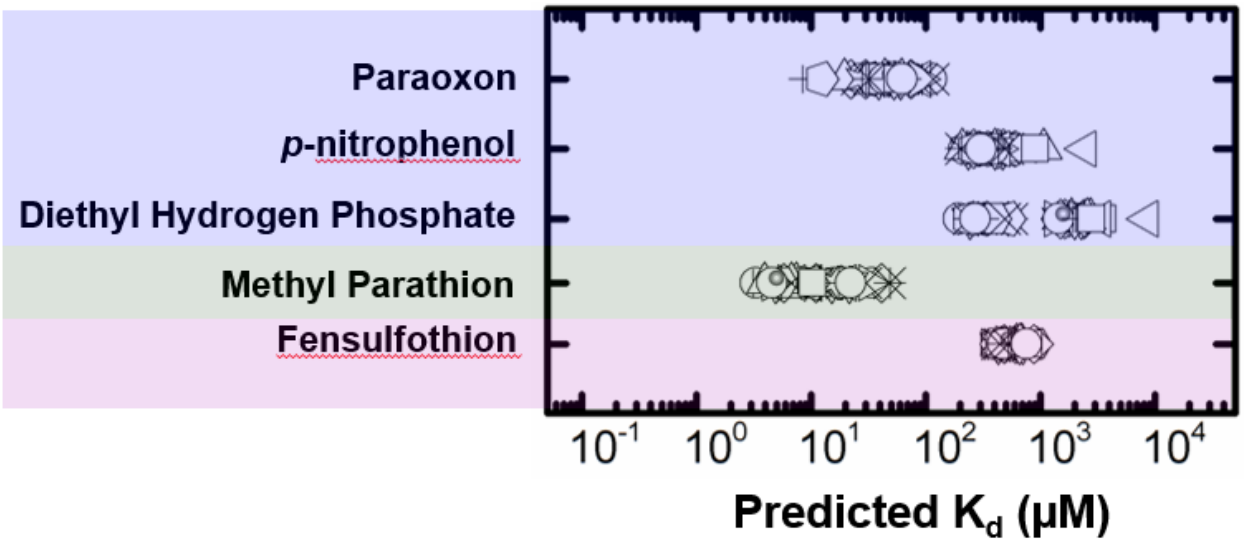

Figure 2-3: Predicted organophosphate binding to DNA using AutoDock 4.2 with 50 unique, 10 bp randomly generated sequences.

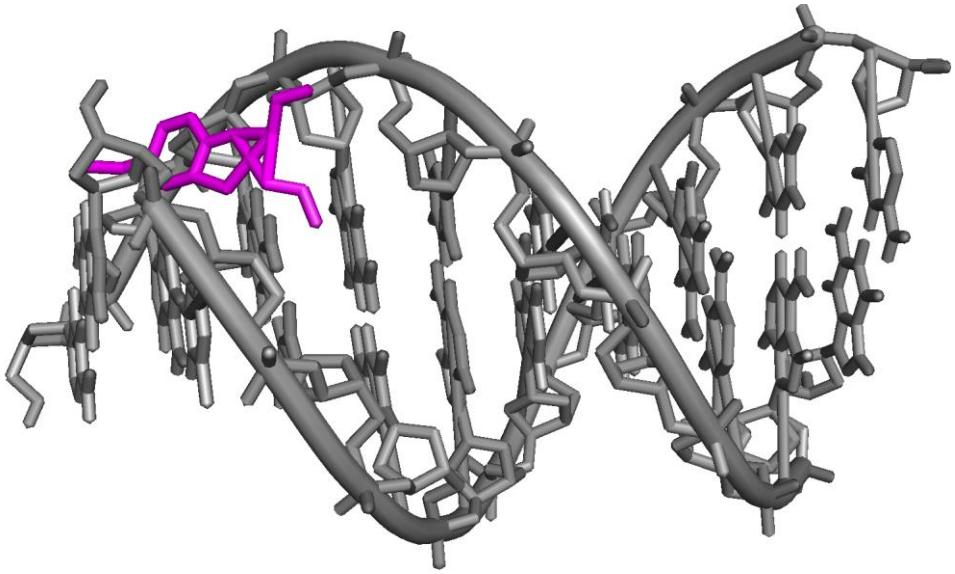

Figure 2-4: An example of the docked conformation of Paraoxon to DNA

Each shape in (Figure 2-2) represents a different DNA sequence which makes it possible to follow a particular DNA sequence. After careful inspection, it becomes apparent that some DNA sequences bind one substrate better than another. With this information, several sequences would be chosen for experimental validation. Since it would be time consuming and would consume a significant amount of resources, we sought three sequences out of the possible fifty sequences for experimental validation. The three sequences we chose are named seq 1 (CAGGTTGCAG), seq 2 (GAATCTTCGG), and seq 3 (CCTAAAAGAG). They were chosen based on paraoxon. Seq 1 had the highest affinity, seq 3 had moderate affinity, and

seq 2 had the weakest affinity for paraoxon. The sequences had low hybridization melting temperatures which would make the 10 bp sequences unstable near room temperature. DNA targets are 20 bp concatenations, DNA1, DNA2, DNA3 of the 10 bp random sequences, seq 1, seq 2, seq 3 to increase their stability. GC content was also examined to avoid sequence bias. These results are shown in (Table 2-1).

Sequences	$T_{m,\ hybridized}$ (°C)	% GC Content	Predicted K_d				
			Paraoxon	Diethyl hydrogen phosphate	*p*-nitrophenol	Methyl parathion	Fensulfothion
Seq 1 5' (CAGGTTGCAG) 3' DNA1 5' $(CAGGTTGCAG)_2$ 3'	29 60.4	60%	11.58	1746.75	181.72	57.63	11.2
Seq 2 5' (GAATCTTCGG) 3' DNA2 5' $(GAATCTTCGG)_2$ 3'	27 53	50%	61.66	267.98	301.61	83.56	12.39
Seq 3 5' $(CCTAAAAGAG)_2$ 3' DNA3 5' $(CCTAAAAGAG)_2$ 3'	20.5 47.8	40%	27.41	2850.56	430	79.44	27.41

Table 2-1: Three chosen DNA sequences named DNA1, DNA2, DNA3 are chosen for experimental validation. Shown here are their DNA sequences, melting temperatures when hybridized, GC content, and their predicted dissociation constants according to AutoDock 4.2.

2.4.2 MICROSCALE THERMOPHORESIS

In order to determine the dissociation constant of DNA1, DNA2, DNA3 to the various organophosphates and two byproducts, MST measurements have been performed. After measurement, the F_{norm} values

were converted into fraction bound for determination of dissociation constants. Buffer and DNA concentrations are kept constant throughout the experiment. The fraction bound (FB) is calculated using $FB = (F_{norm} - F_{norm\ (unbound)})/(F_{norm\ (bound)} - F_{norm\ (unbound)})$.[36] $F_{norm\ (unbound)}$ is given when the substrate concentration is low and $F_{norm\ (bound)}$ is given when the substrate concentration is high. The binding data was fitted to a Hill function (n = 1) using Origin Pro. When the hill constant is equal to 1, the binding is non cooperative meaning the addition of substrate does not affect the overall binding either increasing the probability of binding or decreasing the likelihood of another to bind. All binding measurements were conducted as triplicates and error is shown in the plotted figures. These results are depicted in (Figure 2-5) and (Table 2-2).

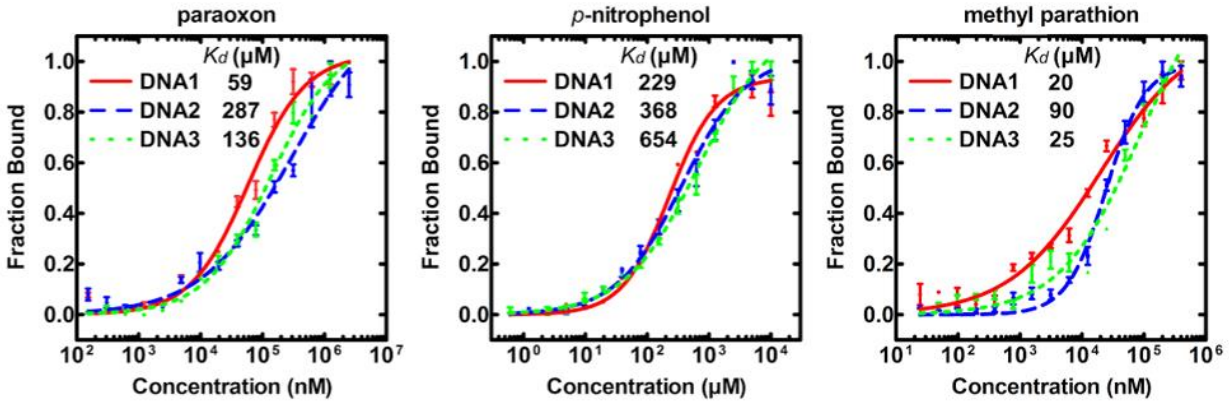

Figure 2-5: The sigmoidal binding curves of organophosphates methyl parathion and paraoxon, as well as the paraoxon byproduct, p-nitrophenol to DNA1, DNA2, DNA3. These curves were fit using Hill Fit function to determine binding dissociation constants.

Sequences	Paraoxon (K_d in μM)		*p*-nitrophenol (K_d in μM)		Methyl parathion (K_d in μM)	
	Nanotemper (MST)	Autodock (10 bp)	Nanotemper (MST)	Autodock (10 bp)	Nanotemper (98%MST+2%DMSO)	Autodock (10 bp)
Seq 1 5' (CAGGTTGCAG) 3'		11.58		181.72		57.63
DNA1 5' $(CAGGTTGCAG)_2$ 3'	58.8 ± 6.2 n=0.94 ± 0.07		229.2±22.9 n=1.13±0.10		20.0±2.3 n=0.58±0.05	
Seq 2 5' (GAATCTTCGG) 3'		61.66		301.61		83.56
DNA2 5' $(GAATCTTCGG)_2$ 3'	286.9±13.8 n=0.61±0.07		368.1±20.1 n=0.82±0.08		90.4±4.4 n=0.66±0.07	
Seq 2 5' $(CCTAAAAGAG)_2$ 3'		27.41		430		79.44
DNA3 5' $(CCTAAAAGAG)_2$ 3'	135.9±12.7 n=0.82±0.06		654.0±50.2 n=0.73±0.05		24.8±2.0 n=1.37±0.12	

Table 2-2: The dissociation constants obtained from both MST and AutoDock for paraoxon, methyl parathion and p-nitrophenol to DNA1, DNA2, DNA3

Inferring from the data, only three out of the total 5 planned substrates were successful. Diethyl hydrogen phosphate and fensulfothion binding data were not able to be obtained using this method. This could be due to non-binding or conformational effects to DNA structure. The dissociation

constants for the successful assays follow similar trends with regards to binding. For example, in AutoDock, for paraoxon, the weakest, moderate and strongest binder was DNA2, DNA3, and DNA1 respectively. This matches the experimental dissociation constants found using MST. The same type of trend applies to *p*-nirophenol and methyl parathion. This means that the predicted values, while not matching exactly with the experimental values, correlations can still be drawn for each substrate and DNA.

2.4.3 FLUORESCENCE STUDIES

Methylene blue (MB) is a phenothiazinium dye that interacts with DNA primarily by intercalation. MB fluorescence is efficiently quenched upon binding to DNA with no shifts in the emission spectrum. This type of interaction between DNA and MB can be visualized in (Figure 2-6).

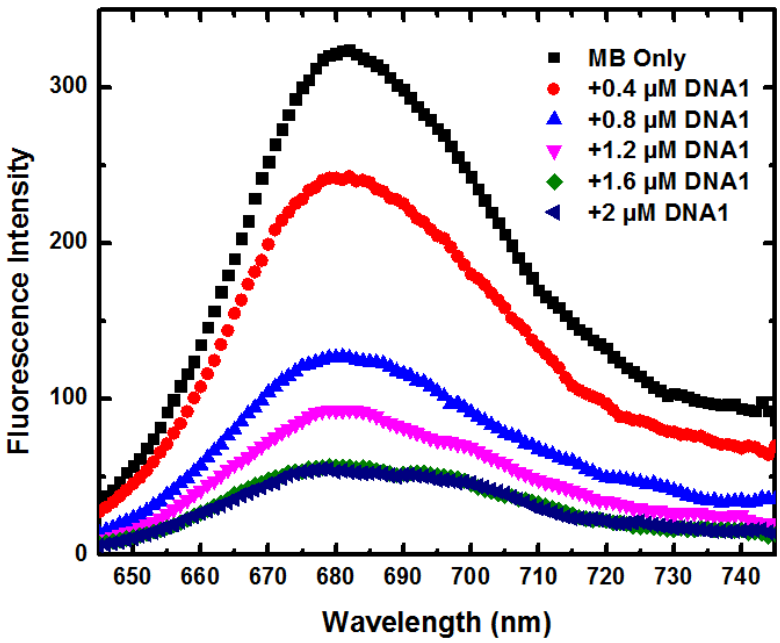

Figure 2-6: Fluorescence emission curve of methylene blue only followed by a constant concentration of methylene blue with increasing concentrations of DNA1.

This decrease is a result of the changes in the excited state electronic structure in combination with the electronic interactions with the DNA+MB complex.[32] When OP or byproduct is added to the DNA+MB solution, if the fluorescence of MB+DNA+substrate is increased, this increase in fluorescence is directly related to the release of MB as a consequence of substrate binding. This phenomenon is utilized for the determination of dissociation constants. Emission curves are shown in (Figure A-1), (Figure A-2), (Figure A-3), and (Figure A-4).

In this set of measurements, only four out of the total 5 planned substrates were successful. In order to elucidate the fluorescence quenching mechanism, the modified Benesi-Hildebrand equation was used. This equation is seen in (figure 2-7).

$$\frac{1}{F - F_0} = \frac{1}{(K_a LQ[MB - DNA]_0)[Substrate]} + \frac{1}{(LQ[MB - DNA]_0)}$$

Figure 2-7: The modified Benesi-Hildebrand equation

Where F and F_0 represent the fluorescence signals in the absence and presence of substrate, $[MB\text{-}DNA]_0$ and [Substrate] represent the initial concentration of MB-DNA complex and substrate concentration, L is the instrumented constant, K_a is formation constant of the Substrate-DNA complexes. By plotting of $1/(F\text{-}F_0)$ vs. 1/[Substrate], K_a can be obtained from the slope and intercept of the resultant linear plots. The linear plots are shown in (Figure 2-8) and compiled data is shown in (Table 2-3).

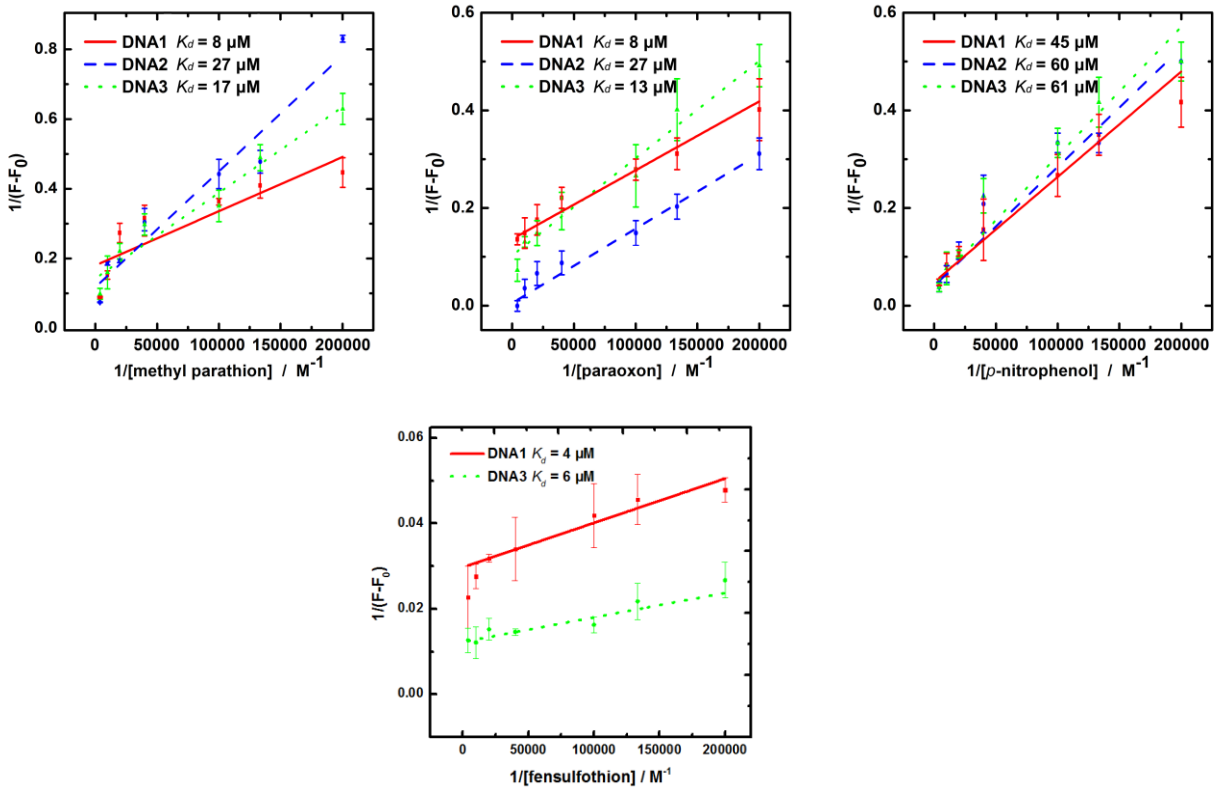

Figure 2-8: Plotting $1/(F-F_0)$ vs. 1/[Substrate] of the recorded fluorescence data using methylene blue to determine the dissociation constant of methyl parathion (top left) , paraoxon (top center) , p-nitrophenol (top right) and fensulfothion (bottom center) following the Benesi-Hildebrand equation

Sequences	Paraoxon (K_d in µM)			*p*-nitrophenol (K_d in µM)		
	Nanotemper (MST)	Methylene Blue	Autodock (10 bp)	Nanotemper (MST)	Methylene Blue	Autodock (10 bp)
Seq 1 5' (CAGGTTGCAG) 3' **DNA1** 5' $(CAGGTTGCAG)_2$ 3'	58.8 ± 6.20 n=0.94±0.07	7.54±0.74	11.58	229±22.9 n=1.13±0.10	44.6±4.75	182
Seq 2 5' (GAATCTTCGG) 3' **DNA2** 5' $(GAATCTTCGG)_2$ 3'	287±13.8 n=0.61±0.07	27.3±2.62	61.66	368±20.1 n=0.82±0.08	59.9±5.31	302
Seq 2 5' $(CCTAAAAGAG)_2$ 3' **DNA3** 5' $(CCTAAAAGAG)_2$ 3'	136±12.7 n=0.82±0.06	13.0±1.37	27.41	654±50.2 n=0.73±0.05	61.2±6.42	430

Sequences	Methyl parathion (K_d in µM)			Fensulfothion (K_d in µM)	
	Nanotemper (98%MST+2% DMSO)	Methylene Blue	Autodock (10 bp)	Methylene Blue	Autodock (10 bp)
Seq 1 5' (CAGGTTGCAG) 3' **DNA1** 5' $(CAGGTTGCAG)_2$ 3'	20.0±2.30 n=0.58±0.05	8.44±0.63	57.6	4.40±0.36	11.2
Seq 2 5' (GAATCTTCGG) 3' **DNA2** 5' $(GAATCTTCGG)_2$ 3'	90.4±4.40 n=0.66±0.07	27.4±2.43	83.6		12.39
Seq 2 5' $(CCTAAAAGAG)_2$ 3' **DNA3** 5' $(CCTAAAAGAG)_2$ 3'	24.8±2.00 n=1.37±0.12	16.8±1.64	79.4	5.72±0.28	27.41

Table 2-3: The dissociation constants obtained from both MST, Methylene Blue, AutoDock for paraoxon, p-nitrophenol, methyl parathion and fensulfothion to DNA1, DNA2, DNA3.

Calculated dissociation constants for the successful assays again follow similar trends with regards to binding. For instance, in AutoDock, for *p*-nitrophenol, the weakest, moderate and strongest binder was DNA3, DNA2, and DNA1 respectively. This matches the experimental dissociation

constants found using MST. The same type of trend applies to paraoxon and methyl parathion. As for fensulfothion, only two out of the three binding constants were able to be calculated. This may be an isolated occurrence that will be explored further in later studies. Overall, these experimentally determined values are a good indication of the binding affinity OPs and two intermediates can have to DNA.

2.4.4 CIRCULAR DICHROISM

Circular dichroism was performed with the intention of observing the binding that we have seen through the two other techniques and its manifestation in conformational changes in DNA. The CD spectra of synthetic oligonucleotides depends on primary sequence. Notably, CD spectra are well conserved. B-form DNA is marked by four bands, a positive band at 275 nm due to base stacking and a negative 245 nm band due to helicity. These are the most sensitive bands for DNA binders.[37] There are two additional peaks, a negative 210 nm and a positive positive peak near 220 nm.[38] The 210 nm peak arises from the β-N-glycosidic linkage that exists between the nitrogenous base and the deoxyribose sugar and 220 nm peak represents hydrogen bonding occurring between the nitrogenous bases of opposite strands.[39] Successful CD using paraoxon, p-nitrophenol, diethyl hydrogen

phosphate, methyl parathion, and fensulfothion are presented in (Figure 2-9), (Figure 2-10), (Figure 2-11), (Figure 2-12) and (Figure 2-13).

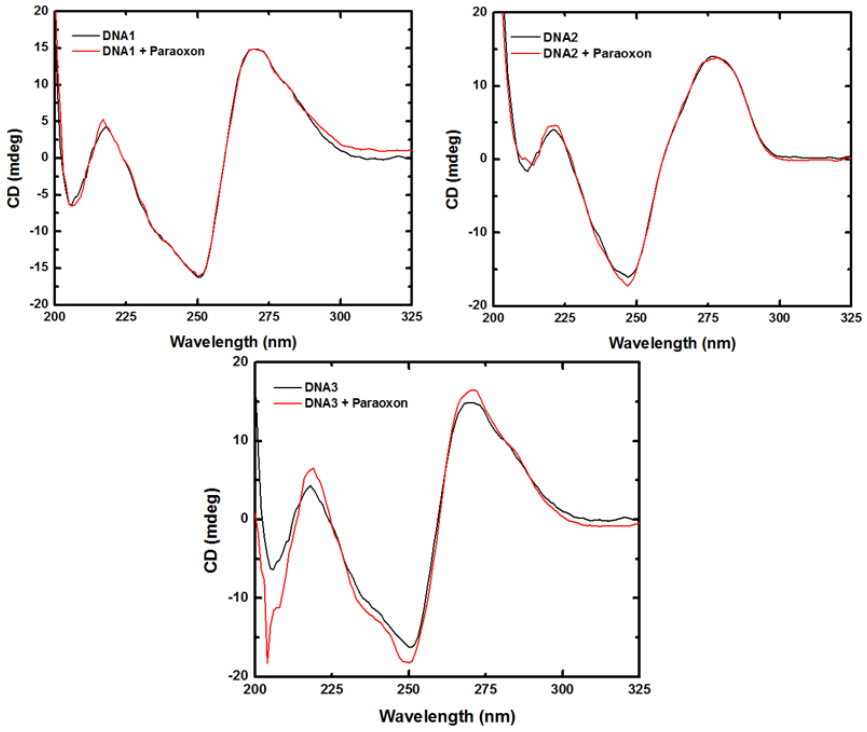

Figure 2-9: Circular dichroism spectra of DNA1 (top left), DNA2 (top right), DNA3 (bottom center) with paraoxon.

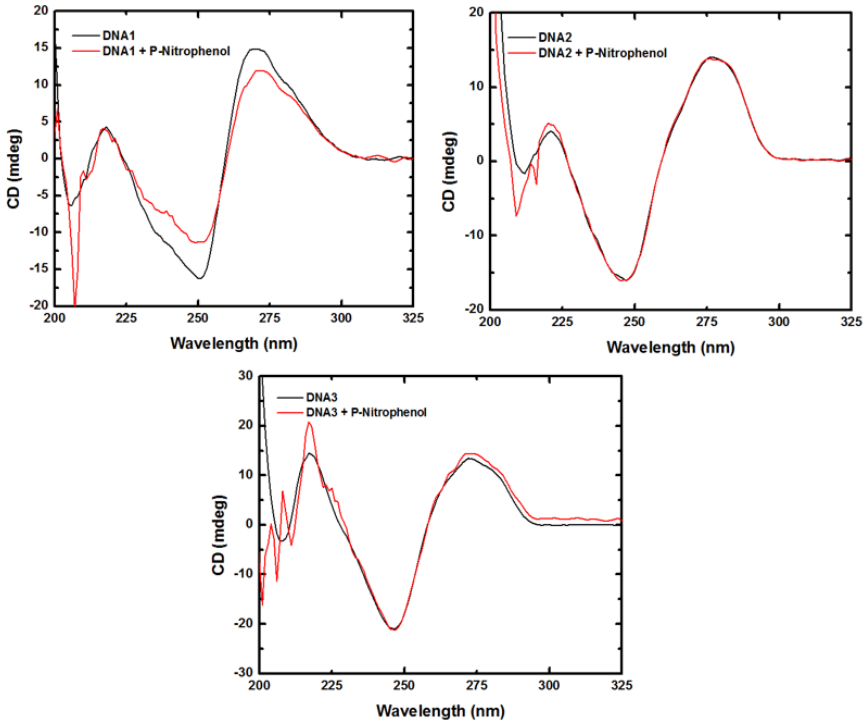

Figure 2-10: Circular dichroism spectra of DNA1 (top left), DNA2 (top right), DNA3 (bottom center) with p-nitrophenol.

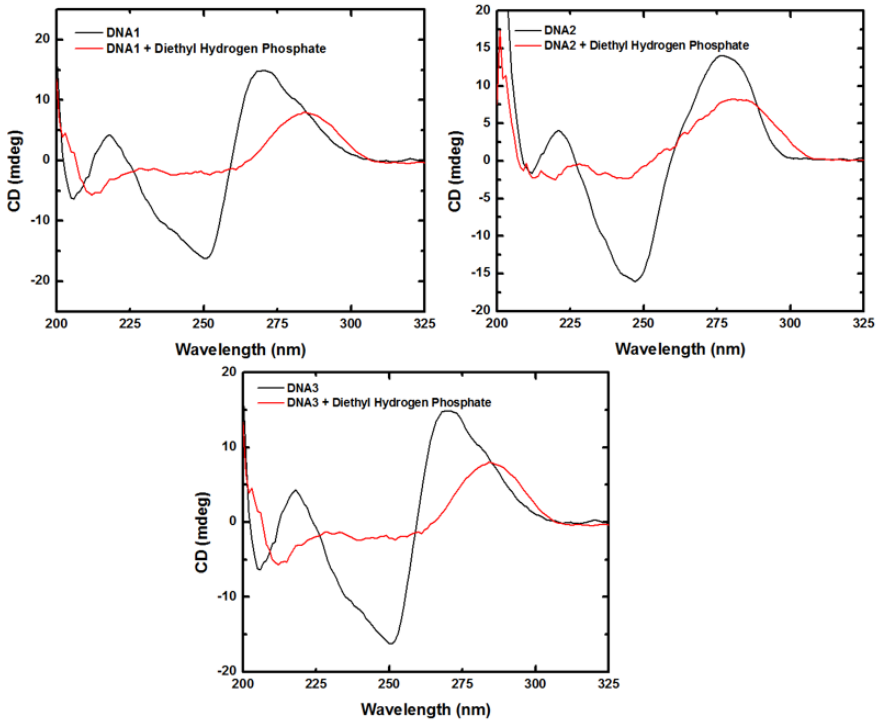

Figure 2-11: Circular dichroism spectra of DNA1 (top left), DNA2 (top right), DNA3 (bottom center) with diethyl hydrogen phosphate.

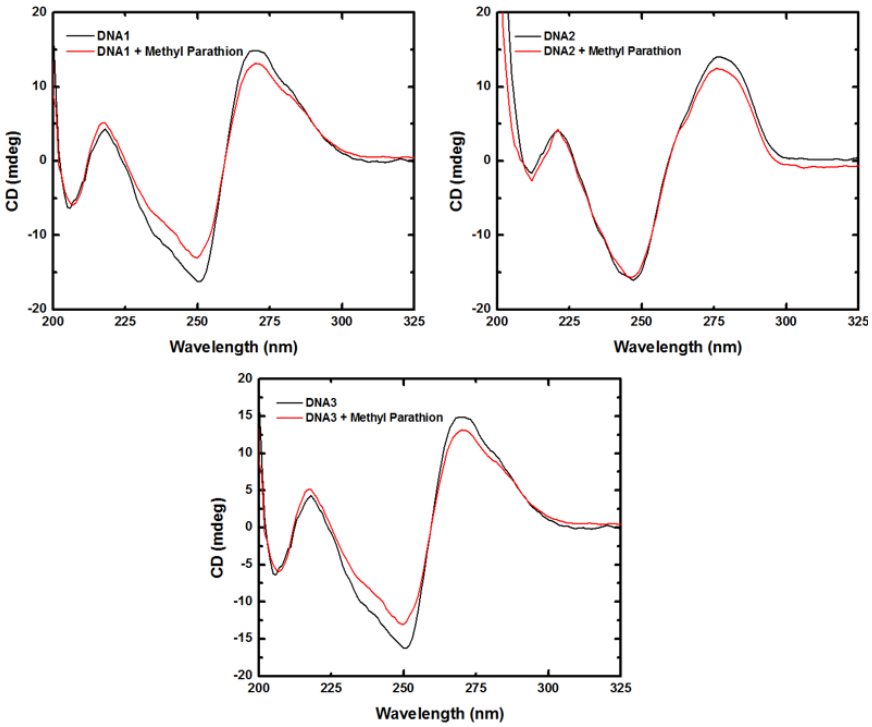

Figure 2-12: Circular dichroism spectra of DNA1 (top left), DNA2 (top right), DNA3 (bottom center) with methyl parathion.

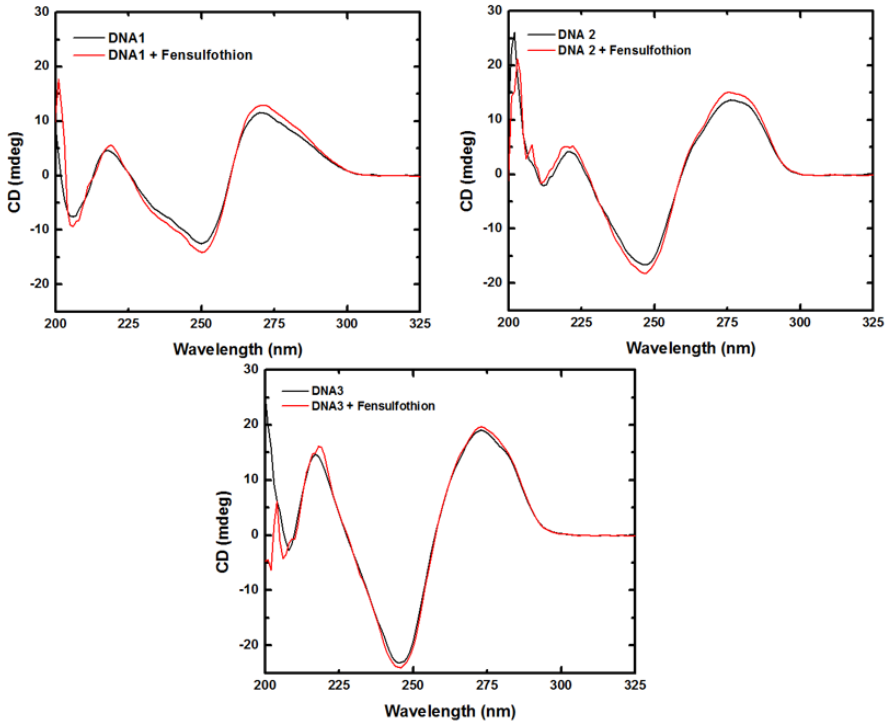

Figure 2-13: Circular dichroism spectra of DNA1 (top left), DNA2 (top right), DNA3 (bottom center) with fensulfothion.

As seen in (Figure 2-9), (Figure 2-10), (Figure 2-11), (Figure 2-12) and (Figure 2-13), shifts in band position and intensity are a direct result of conformational transitions of DNA.[40] If a molecule binds via intercalation, the weakening of the π- π stacking of the base pairs loosens the double helix conformation.[41] In consequence, there would be a decrease in the intensity due to disruption of the positive band for base stacking interaction near 275 nm as well as a decrease in the intensity of the negative band around 245 nm due to helix disruption. [42] DNA unwinding allows the sugar-phosphodiester

backbone to span the intercalator while still maintain the link between flanking base pairs. This type of intercalation is seen for DNA1 with p-nitrophenol (Figure 2-10), methyl parathion (Figure 2-12) and DNA3 with methyl parathion (Figure 2-12). A slight modification to this type of intercalative binding is seen when only a decrease in the base stacking band at 275 nm occurs, indicating separation of the bases. This is observed when DNA2 interacts with methyl parathion (Figure 2-12) and is seen as a "weaker" type of intercalation as it does not perturb the helicity of DNA. Bathochromic (red or higher wavelength) shifts or hypsochromic (blue or lower wavelength) shifts in the CD spectra indicate major changes in the secondary structure conformation of DNA. Major changes in the DNA structure are seen in the interaction between diethyl hydrogen phosphate and DNA1, DNA2, DNA3 (Figure 2-11). Red shifting of all the bands indicates that binding is occurring but it is affecting the overall structure of DNA. This might explain why measurements using the earlier two methods were not successful. In the situation where the intensity after the addition of substrate leads to an increase of the 275 nm band, this indicates enhancement of base stacking while the decrease in the 245 nm band suggests it became a more highly wound form of B-DNA.[43] This type is seen for DNA1 and DNA2 with fensulfothion (Figure

2-13) and DNA3 with paraoxon (Figure 2-9). There is a special case in DNA3 with paraoxon where the 210 nm peak decreases as well. This indicates that it may be a conformational change from B-form to A-form which is a tighter form of DNA. Groove binders do not perturb the CD spectrum significantly.[44] Groove binding can be seen for DNA1 and DNA2 paraoxon (Figure 2-9), DNA2 and DNA3 for *p*-nitrophenol (Figure 2-10), and DNA3 for fensulfothion (Figure 2-13). A table that summarizes these results are in (Table 2-4).

DNA Sequence	Paraoxon	*p*-nitrophenol	Diethyl hydrogen phosphate	Methyl Parathion	Fensulfothion
DNA1	Groove Binding	Intercalation	Major DNA conformational change	Intercalation	Highly wound form DNA
DNA2	Groove Binding	Groove Binding	Major DNA conformational change	"weak" Intercalation	Highly wound form DNA
DNA3	Highly wound form DNA	Groove Binding	Major DNA conformational change	Intercalation	Groove Binding

Table 2-4: A table summarizing the results of the circular dichroism studies

CHAPTER 3: DETERMINATION OF SEQUENCE DEPENDENT BINDING

3.1 METHODS TO ELUCIDATE THE CAUSE OF SEQUENCE DEPENDENT BINDING

Evidence from the previous chapter supported our hypothesis of the ability of OPs and byproducts to bind to DNA. It was initially apparent from the fifty random DNA sequences we chose to screen using Autodock had different affinities to DNA. This was further supported by the experimental data from Nanotemper, fluorescence studies and circular dichroism. This next chapter will examine the presence of sequence dependent binding for our main OP of study, paraoxon.

Reiterating the main objective, the goal of tuned DNA scaffolds that promote beneficial substrate interactions requires differential binding of substrates to different DNA sequences. By identifying the source of differential binding, tuned substrate interactions to DNA would become a reality. Methods that are used in this section are Fourier transform-infrared spectroscopy, fluorescence studies and circular dichroism.

Fourier transform-infrared spectroscopy is a different method to determine the binding of paraoxon. Pre-established bands corresponding to confined regions on DNA infrared spectra indicate possible binding locations on the DNA structure. By monitoring band shifts and intensity changes, information about the binding event will be revealed.

Fluorescence studies can be reused in an analogous manner to examine binding by monitoring variations in the emission spectra with increasing concentrations of paraoxon. In order to pinpoint binding regions, two additional DNA probes, one that binds exclusively to the major groove and one that binds exclusively to the minor groove are added. This will grant further insight into which mode(s) of DNA binding paraoxon may appropriate to.

Finally, circular dichroism can also be re-utilized in determining the binding of OPs and byproducts to specific repeat sequences rather than random sequences. The repeat sequences include $(A)_{20}$, $(G)_{20}$, $(AT)_{10}$, $(GC)_{10}$, $(TC)_{10}$, and $(TG)_{10}$ providing good coverage of the possible binding locations.

3.2 METHODS

3.2.1 Chemicals

Paraoxon-Ethyl, Methylene Blue, Hoechst 33258, and Methyl Green were purchased from Sigma-Aldrich (St. Louis, MO). Oligonucleotides DNA1, DNA2 and DNA3, $(A)_{20}$, $(G)_{20}$, $(AT)_{10}$, $(GC)_{10}$, $(TC)_{10}$, and $(TG)_{10}$ were purchased from Integrated DNA Technologies (IDT).

3.2.2 Experimental Set Up

FT-IR Spectroscopy

The FT-IR spectra were measured on a Thermo-Nicolet 6700 FT-IR spectrometer via the ATR method over the spectral range of 1800-800 cm^{-1} with a resolution of 4 cm^{-1} and 100 scans. The beamsplitter component was a KBr and the sample detector was a DTGS KBr. FT-IR spectra were recorded before and after addition of paraoxon. Phosphate buffer was used and the measurements were carried out at room temperature. Background spectra was also collected before each measurement. A spectrum of buffer solution was also measured and subtracted from the spectra of the DNA and DNA-substrate complexes. Tabulated results in a comma separated value file were then exported for use in excel.

Fluorescence Studies

Fluorescence studies were done using a BioTek Synergy 4 microplate reader. Each plate contained 96 to 384 well plates that hold a maximum of 100 µL per well. DNA1, DNA2, DNA3 were prepared by denaturation then a series of steps involving cooling. The probe that was used was methylene blue (10 µM), Hoechst 33258 (5 µM), methyl green (5 µM). Different DNA1, DNA2, DNA3 concentrations were used; 2.5 µM for methylene blue and 10 µM for Hoechst 33258 and methyl green. DNA1, DNA2, DNA3 was added to well containing either methylene blue, Hoechst 33258 or methyl green. This was followed by multiple wells with DNA and probe where different concentrations of paraoxon were 10, 60, 110, 160, 210, 260, 310, 360, and 410 µM of paraoxon. Concentrations of paraoxon used for the methylene blue study are explained in the last chapter. After thorough mixing through pipette, these solutions were inserted into the plate reader where they were shaken for 8 seconds then allowed 8 minutes to equilibrate. The fluorescence emission spectra were then measured by using excitation wavelengths of 615 nm, 346 nm, and 633 nm in the range of 645 to 745 nm, 376 to 576 nm, and 663 to 800 nm for methylene blue, Hoechst 33258 and methyl green respectively. A blank containing buffer PB for methylene blue and Tris-HCl for Hoechst 33258 and Tris-HCl was subtracted to correct background fluorescence

accordingly. Tabulated results were exported in an excel file where they would be further analyzed.

Circular Dichroism Spectroscopy

Circular dichroism (CD) measurements were obtained on a Jasco J-815 CD spectrometer. These were done under a constant stream of nitrogen to purge water vapor from the sample chamber. Continuous accumulation of CD spectra at wavelengths 500 nm to 190 nm was taken. $(A)_{20}$, $(G)_{20}$, $(AT)_{10}$, $(GC)_{10}$, $(TC)_{10}$, and $(TG)_{10}$ spectra without any OPs or byproducts were first measured. The concentration of DNA was 40 µM. This was then followed by the addition of paraoxon up to 10 mM. The software used was provided by Jasco for instrument control and data acquisition. The scans were done at room temperature in phosphate buffer using a 1 mm quartz cuvettes. A spectrum of phosphate buffer solution was also recorded and subtracted from the spectra of DNA and DNA-substrate complexes. For each spectrum, 5-10 runs were averaged with a 5 minute equilibration time before each scan. Values for the CD spectra were exported in a comma separated value file for use in excel.

3.3 RESULTS & DISCUSSION

3.3.1 FT-IR Spectroscopy

The infrared spectra of DNA contains useful information regarding OPs and their byproducts specific binding to locations on the DNA helix. Peaks can be associated with specific interaction to the phosphate skeleton and base pairs. [43] Ring vibrations of the nitrogenous bases (C=O, C=N stretching) and PO_2 backbone stretching vibrations (symmetric and asymmetric vibrations) are confined to a specific region in the infrared spectrum.[45] When OPs and their byproducts interact with DNA, shifts in peak position and intensity can be observed. Infrared spectra for DNA1, DNA2, DNA3 with paraoxon are seen in (Figure 3-1) and (Figure 3-2).

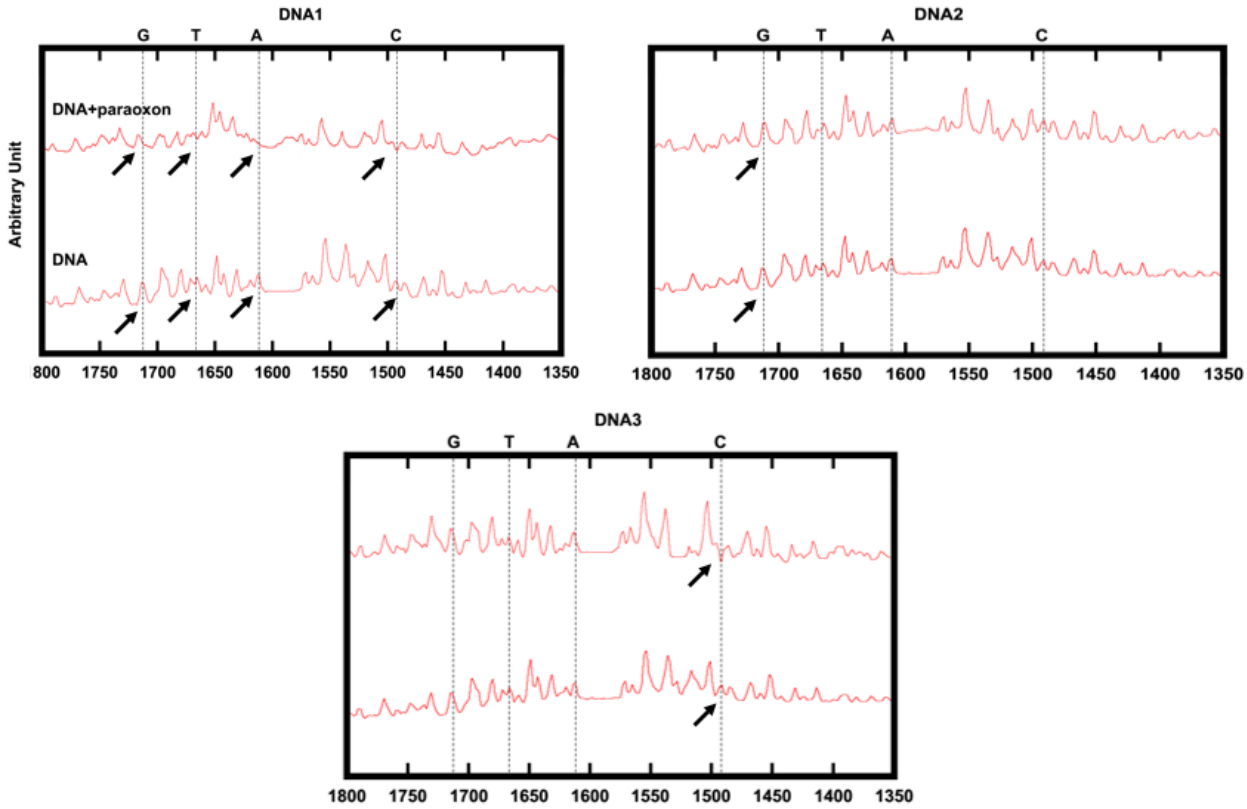

Figure 3-1: FT-IR spectra with a constant concentration of DNA1 (top left), DNA2 (top right), and DNA3 (bottom center) from 1800 cm^{-1} to 1300 cm^{-1}. DNA with paraoxon is on the first row while DNA only is on the bottom row in each of the plots.

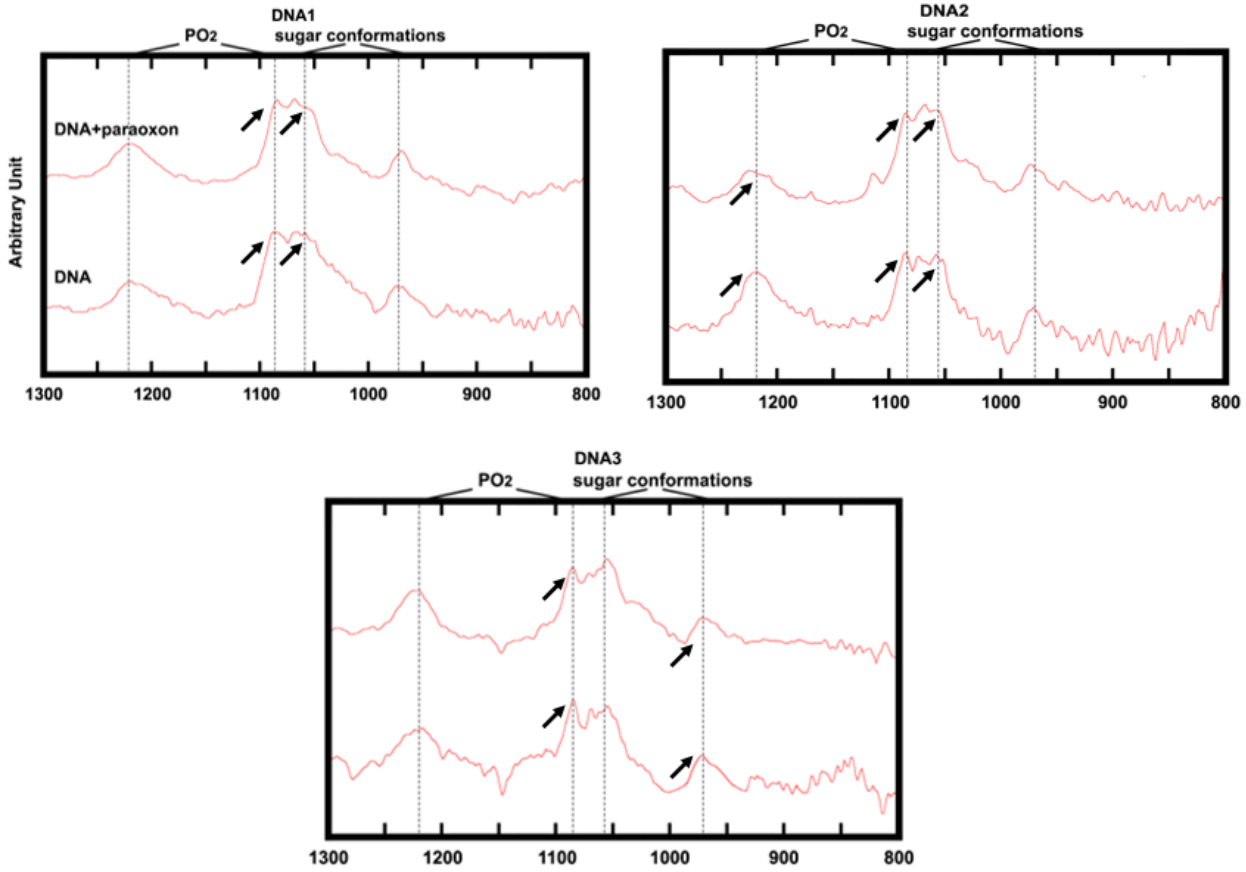

Figure 3-2: FT-IR spectra with a constant concentration of DNA1 (top left), DNA2 (top right), and DNA3 (bottom center) from 1300 cm^{-1} to 800 cm^{-1}. DNA with paraoxon is on the first row while DNA only is on the bottom row in each of the plots.

The band at 1714 cm^{-1} is attributed to guanine (G) in plane stretching vibrations.[46] The band at 1665 cm^{-1} is recognized as vibrations from thymine (T) stretching. The band at 1612 cm^{-1} is associated with adenine (A) base vibrations while the band at 1493 cm^{-1} is due to cytosine (C) vibrations. Sugar-phosphate backbone interactions can be also detected. The bands at 1223 cm^{-}

[1] and 1086 cm^{-1} correspond to phosphate asymmetric and symmetric vibrations. Specifically, 1223 cm^{-1} is considered to be a B-form marker which is attributed to antisymmetric phosphate stretching while the band corresponding A-form DNA is slightly shifted to 1240 cm^{-1}. The bands at 1053 cm^{-1} gives shoulder like appearance due to sugar vibrations. The band at 970 cm^{-1} is also associated with sugar conformation vibrations. Shifts in the absorption bands of guanine, adenine, cytosine, thymine are accompanied by intensity variations when paraoxon is added to the sample. For example, in DNA1 with paraoxon, there is a blue shift to lower wavenumber in the guanine band, decrease in intensity of the thymine band, loss of the band corresponding to adenine, and red shift to a higher wavenumber for the cytosine band. In the phosphate sugar backbone bands, there are slight red and blue shifts in each of the corresponding bands. Based on these observations, it is clear that paraoxon can intercalatively bind to the bases as well as the groove. [45] In DNA2 with paraoxon, there is a red shift in the bands related to guanine base binding. From the binding spectra of paraoxon to DNA2 in phosphate sugar backbone bands, there are shifts in the phosphate, sugar conformations for both the intensity and position of the bands. It can be concluded that paraoxon can interact with DNA2 by intercalation and groove

binding. By inspection of the DNA3 bands for paraoxon binding, there is an inversion of the cytosine band. According to the bands corresponding to the phosphate sugar backbone, there are intensity fluctuations. From these observations, it can be concluded that paraoxon can interact with DNA1, DNA2, DNA3 in specific regions.

3.3.2 Fluorescence Studies

Two known DNA groove binders, Hoechst 33258 and Methyl Green (MG), can either binds to the minor groove in A-T rich regions or the major groove respectively.[31] The specificity of these probes towards predefined regions of DNA allows us to identify preferential binding locations. Hoechst 33258 fluorescence is enhanced upon binding to DNA in the emission spectrum. This type of interaction between DNA and Hoechst 33258 can be visualized in (Figure 3-3).

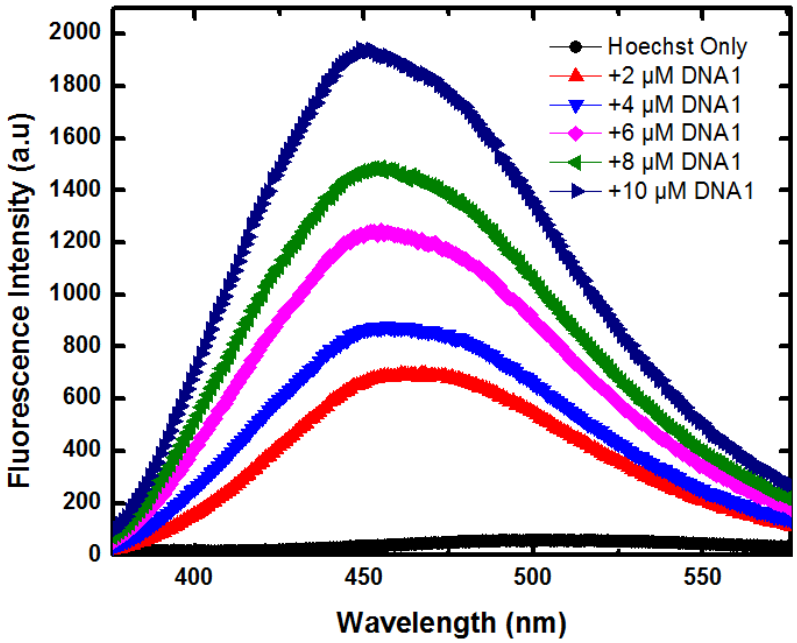

Figure 3-3: Fluorescence emission curve of Hoechst 33258 only followed by a constant concentration of Hoechst 33258 with increasing concentrations of DNA1.

The fluorescence increases due to higher planarity in the grooves of DNA as well as from the protection against solvent collisions.[47] In this assay, the fluorescence emission spectra is observed when a fixed amount of DNA and Hoechst were measured with increasing amounts of organophosphate. Fluorescence intensities gradually decreased with increasing concentration of organophosphate due to competition for groove sites on DNA. Fluorescence emission spectra when paraoxon is added to a constant concentration of DNA and Hoechst 33258 is shown in (Figure 3-4).

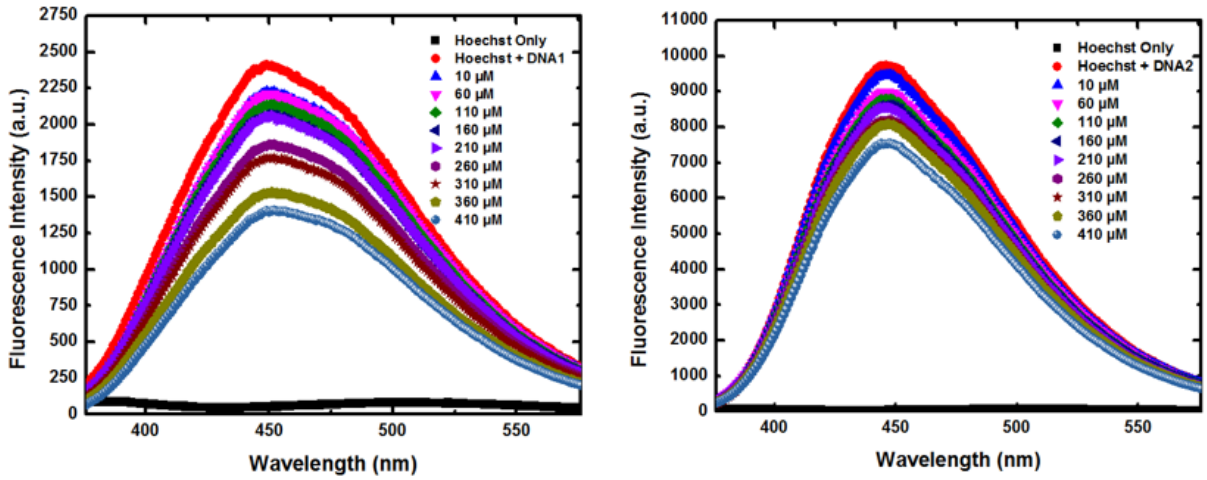

Figure 3-4: Fluorescence emission with a constant concentration of Hoechst 33258 and DNA1 (top left), DNA2 (top right) with increasing paraoxon concentration (10, 60, 110, 160, 210, 260, 310, 360, 410 µM).

The Hoechst 33258 assay was successful for DNA1 and DNA2 with paraoxon. This is in accordance with the data from CD presented earlier. Paraoxon seems to bind to DNA1, DNA2, and DNA3 through intercalation but only DNA1 and DNA2 can bind paraoxon through the minor groove. These results suggest that there could be minor groove binding and intercalative binding for DNA1 and DNA2. Using the modified Benesi-Hildebrand equation, the dissociation constant for DNA could be solved. The curves corresponding to the fluorescence data is found in (Figure 3-5).

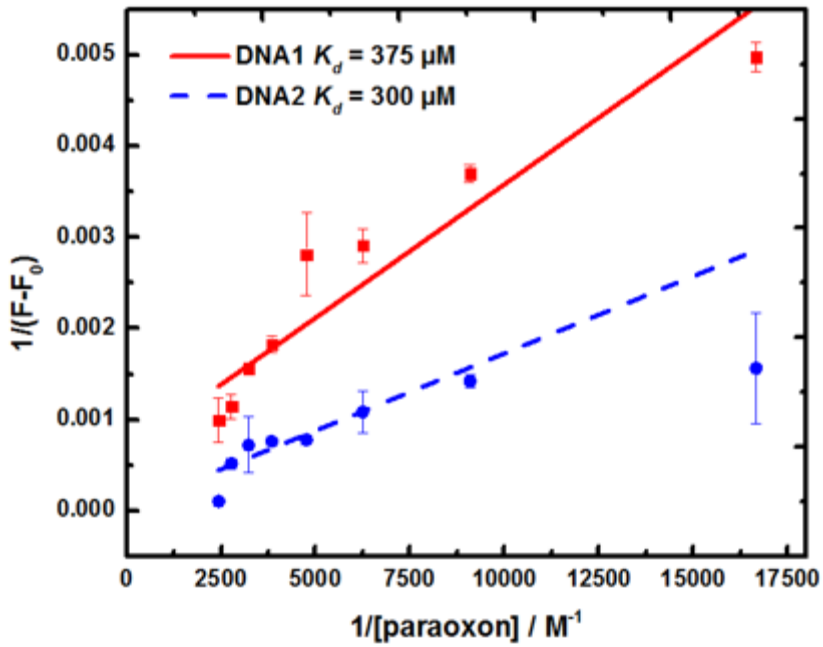

Figure 3-5: Plotting 1/(F-F_0) vs. 1/[Substrate] of the recorded fluorescence data using Hoechst 33258 to determine the dissociation constant of paraoxon following the Benesi-Hildebrand equation

Similarily to Hoechst, MG fluorescence is enhanced upon DNA binding. Interaction between DNA and MG is seen in (Figure 3-6)

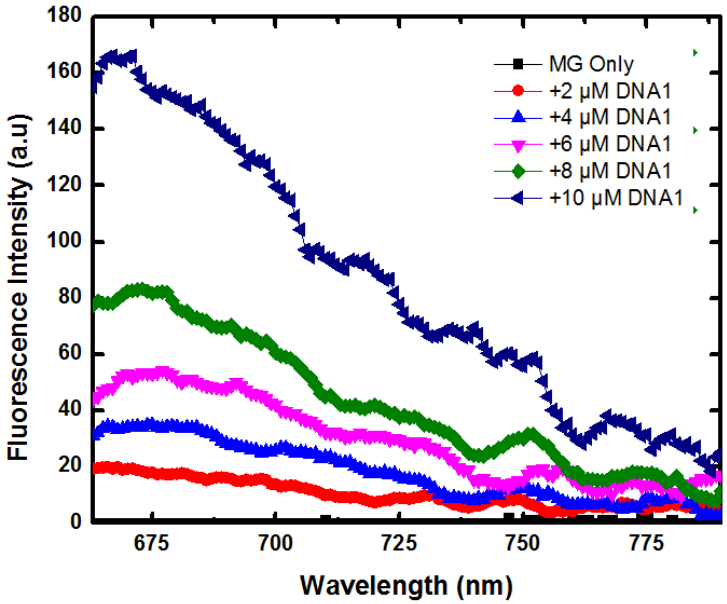

Figure 3-6: Fluorescence emission curve of MG only followed by a constant concentration of MG with increasing concentrations of DNA1.

The emission spectra would again be measured with MG by using a fixed concentration of MG and DNA with increasing paraoxon concentration. This can be seen in (Figure 3-7).

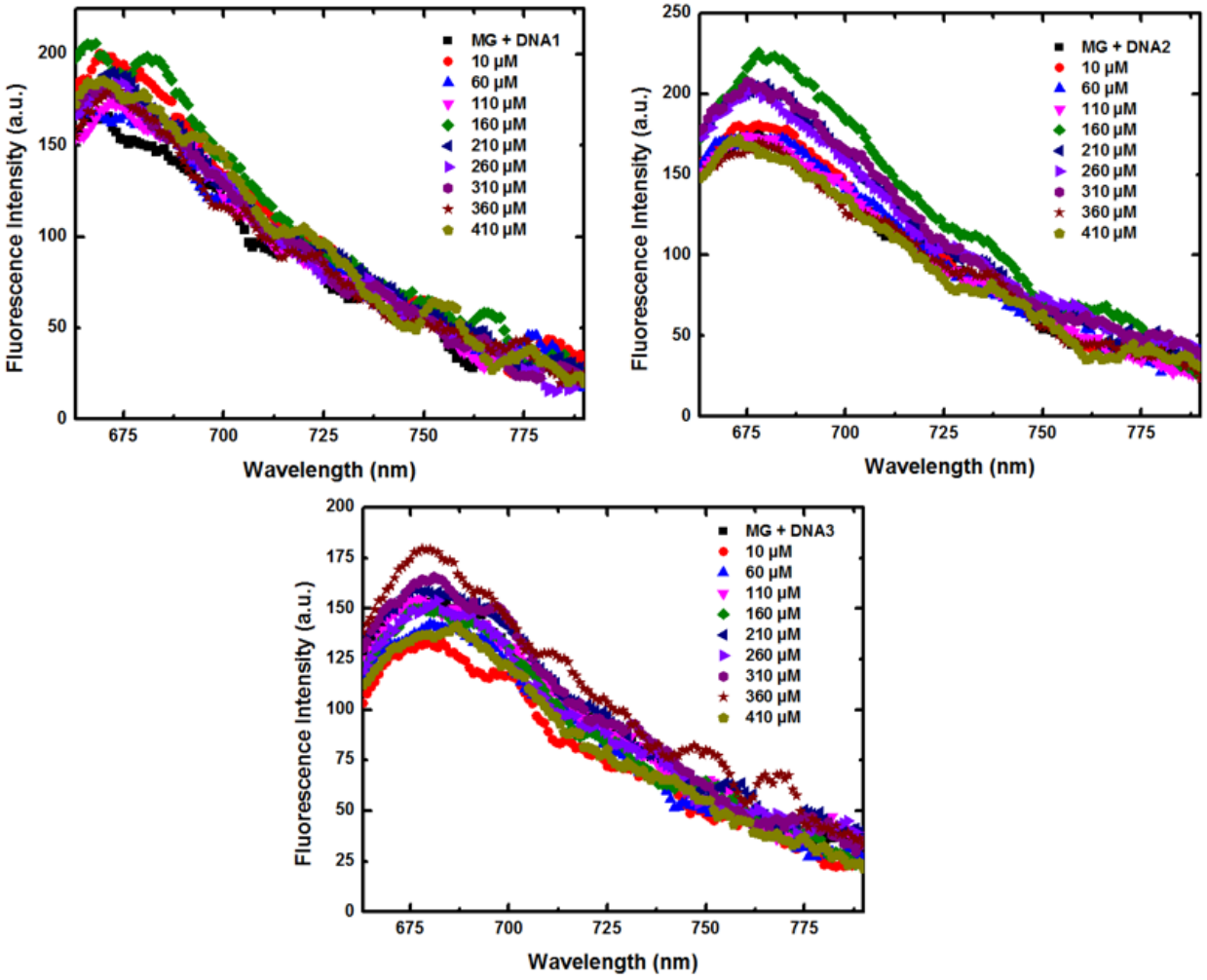

Figure 3-7: Fluorescence emission with a constant concentration of MG and DNA1 (top left), DNA2 (top right), and DNA3 (bottom center) with increasing paraoxon concentration (10, 60, 110, 160, 210, 260, 310, 360, 410 µM).

After paraoxon was added to the MG+DNA mixture, significant quenching did not occur in a concentration dependent manner. This clearly

suggests that paraoxon does not bind to DNA by major groove binding mode.

3.3.3 Circular Dichroism Spectroscopy

In order to finally confirm binding to specific bases, circular dichroism would be performed again with base repeats. When there is bias to a specific repeat, the CD spectra changes. As (A + T) content increases, the negative band becomes deeper and conformational variability increases.[33] The appearance of two positive bands above 250 nm is also apparent for sequences containing exclusively A or T. These can be seen in (Figure 3-8).

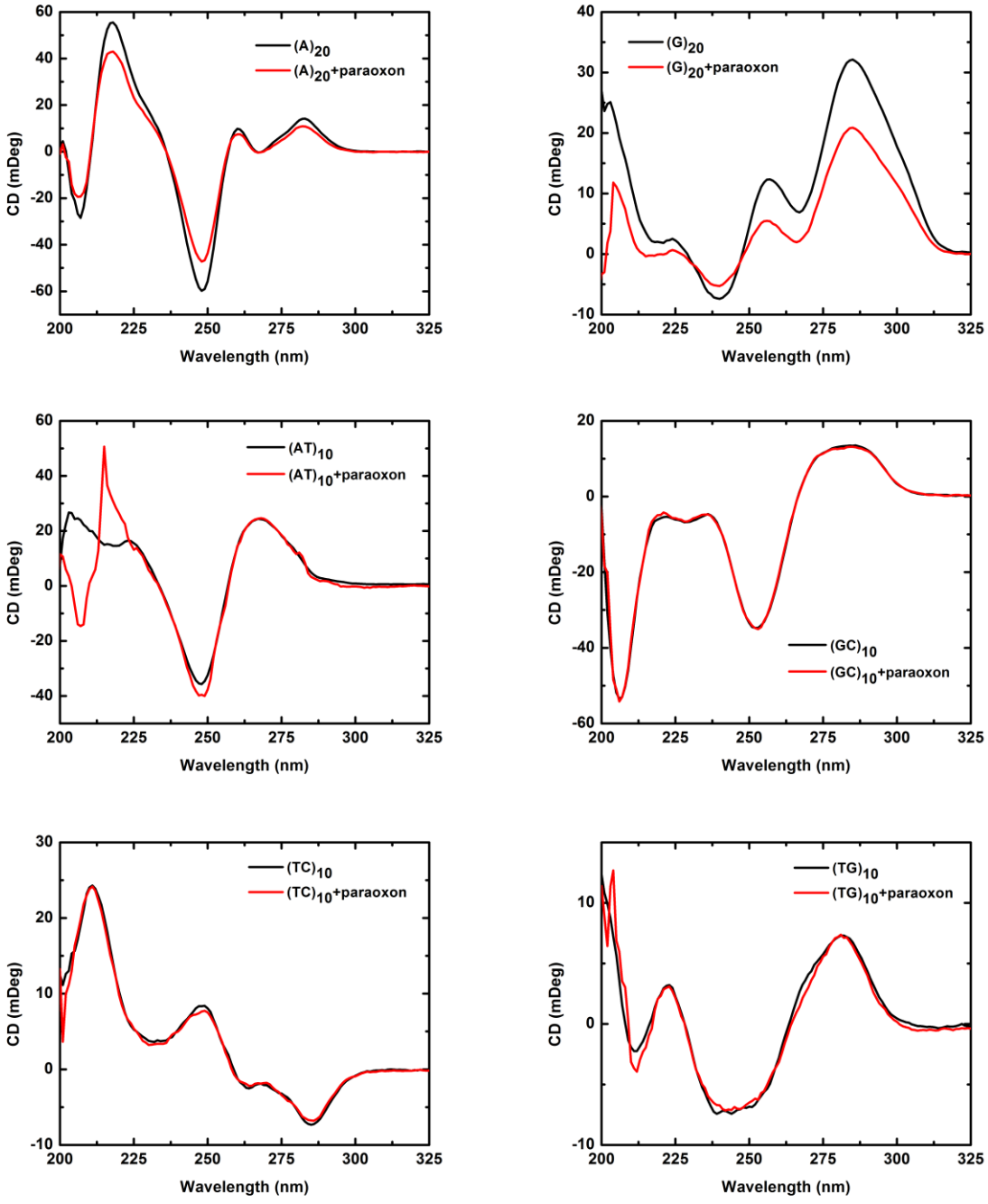

Figure 3-8: Circular dichroism of different DNA repeat sequences of $(A)_{20}$, $(G)_{20}$, $(AT)_{10}$, $(GC)_{10}$, $(TC)_{10}$, and $(TG)_{10}$ only, with subsequent addition of paraoxon with a constant concentration of DNA

Inferred from the CD spectra of the different repeat sequences, intensity changes are triggered upon paraoxon addition. In the adenine rich sequence, a decrease in the negative band near 250 nm and the positive bands near 210 nm, 260 nm and 280 nm signifies binding preference to this region. In the guanine rich sequence, a decrease in the intensity of the positive bands at around 280 nm, 260 nm, 225 nm, and 210 nm as well as the increase in intensity of the negative regions at 260 nm signifies binding preference to this region as well. Based on these two conclusions it seems that repeat sequences of a singular base assists with paraoxon binding. For the alternating repeats, $(AT)_{10}$, $(GC)_{10}$, $(TC)_{10}$, and $(TG)_{10}$, it appears that $(AT)_{10}$ and $(TC)_{10}$ had disruptions to its spectra after paraoxon addition. There is a decrease in the negative peak around 250 nm, a strong induced peak around 215 nm and at 205 nm. This could mean that AT and TC rich regions are preferred areas of binding for paraoxon.

CHAPTER 4: CONCLUSIONS

4.1 CONCLUSIONS and RECOMMENDATIONS

Organophosphates are toxic compounds that need to be degraded in a safe, environmentally friendly behavior. In this study, the goal was to analyze organophosphate binding to DNA in hopes of using it as a nanoscale scaffold to aid the destruction of toxic OPs by enzymatic methods. These interactions between DNA and OP would lead to an overall increase in enzyme activity and catalytic efficiency.

In order to first test if organophosphates can bind to DNA, we used the binding prediction software, AutoDock. This automated software was easy to use and gave us the ability to screen a library of fifty random 20 bp sequences with OPs and their byproducts. From this library we chose three sequences for experimental validation. The first experimental method that was used was microscale thermophoresis. The results would corroborate the findings from AutoDock that OPs and byproducts do bind to DNA and have different affinities based on dissociation constants. In order further to support this narrative, two spectroscopic methods, fluorescence studies involving methylene blue and circular dichroism were also completed. Methylene blue dissociation constants would follow the same trend of weak,

moderate and strong affinities as microscale thermophoresis and AutoDock. Predicted binding results differed from experimental binding constants can be attributed to the differences in the microenvironment of the simulations and the experimental measurements. Experimental binding constants between microscale thermophoresis and fluorescence studies differed as methylene blue measures a very specific mode of binding, intercalation, while microscale thermophoresis can measure multiple modes of DNA binding. Circular dichroism allowed us to verify conformations of binding and whether or not substrate binding altered DNA structure. It was found that conformations did change, and substrate binding sometimes preferred specific regions of binding. Further spectral analysis revealed that diethyl hydrogen phosphate was found to disrupt DNA structure which explains why experimental constants for binding were not obtained for diethyl hydrogen phosphate. These results satisfied our first objective which is that indeed organophosphates do bind to DNA.

From this, we decided to see if OPs could bind in a sequence dependent manner to DNA in order to optimize binding. Further investigation using paraoxon as the target organophosphate was needed. To do so, we used Fourier transform-infrared spectroscopy which is a method

that can determine binding interactions to specified regions on DNA. It was shown that paraoxon can interact to specific DNA bases as well as DNA grooves. From the first chapter, fluorescence studies with methylene blue showed that paraoxon can interact with DNA through intercalation. Based on circular dichroism in chapter 1, it was found that paraoxon could interact by binding to the grooves. In order to investigate the type of groove binding, the next experiments involved a major and minor groove binder, methyl green and Hoechst 33258 respectively. It was found that paraoxon could interact with DNA1 and DNA2 through the minor groove and not DNA3, corroborating the results from circular dichroism in chapter 1. Paraoxon could not interact with the major groove of DNA1, DNA2, or DNA3. The final experiment involved the re-use of circular dichroism with different repeat sequences $(A)_{20}$, $(G)_{20}$, $(AT)_{10}$, $(GC)_{10}$, $(TC)_{10}$, and $(TG)_{10}$. Results demonstrated that paraoxon had a preference towards rich sequences of adenine and guanine as well as a preference towards alternating repeat AT and TC rich sequences.

These sets of experiments lay the groundwork for the use of DNA sequences as a rational design tool to attract toxic compounds and highlight the possibility of DNA based molecular scaffolds for enzymatic degradation

of organophosphates. Using these methods and results generated from organophosphate and DNA binding, the development of rules for DNA sequence design may be possible. If there is variability to preferred DNA sequences, tuning of substrate interactions to cause preferential binding of one substrate towards enzymatic degradation would further support the overall objective of this project. In order to further verify whether the beneficial interactions caused by DNA scaffolds truly do affect catalysis, DNA conjugation of the PTE-S5 enzyme must be done. Further sequence dependence studies using different organophosphates and their intermediates must also be completed. The more rigid structures found in DNA tiles should prove to further enhance OP and byproduct binding by allowing more sequence dependent interactions. DNA tiles, which are specialized complexes of DNA can lead to the possibility of cascade reactions to continue to break down toxic compounds into less toxic compounds. Engineering improved enzymes is a complex task, but this novel method utilizing DNA scaffolds may prove to be one of the more fascinating discoveries in this modern technological age.

AUTHOR INFORMATION

Corresponding Author

*E-mail: iwheeldon@engr.ucr.edu

REFERENCES

1. Bigley, A. N. & Raushel, F. M. Catalytic mechanisms for phosphotriesterases. *Biochim. Biophys. Acta* **1834,** 443–53 (2013).

2. Hossain, M. S. & Sikder, M. T. Potential Human Health Impacts and Medical Treatment of Acute Poisoning with Organophosphorus Pesticides (OPs): A Review. *Science Publishing Group* **3,** 6 (2015).

3. Barnaby, F. *The Role and Control of Weapons in the 1990s*. (Routledge, 2012). at <https://books.google.com/books?id=H8wwRGrD6V4C&pgis=1>

4. Iyer, R., Iken, B. & Leon, A. Developments in alternative treatments for organophosphate poisoning. *Toxicol. Lett.* **233,** 200–206 (2015).

5. Carletti, E. *et al.* Structure-activity analysis of aging and reactivation of human butyrylcholinesterase inhibited by analogues of tabun. *Biochem. J.* **421,** 97–106 (2009).

6. Wingard, L. B. J., Katchalski-Katzir, E. & Goldstein, L. *Immobilized Enzyme Principles: Applied Biochemistry and Bioengineering*. (Elsevier, 2014). at <https://books.google.com/books?id=HTiaBQAAQBAJ&pgis=1>

7. *Organophosphates Chemistry, Fate, and Effects: Chemistry, Fate, and Effects*. (Elsevier, 1992). at <https://books.google.com/books?id=WSkXBQAAQBAJ&pgis=1>

8. Mercey, G. *et al.* Reactivators of acetylcholinesterase inhibited by organophosphorus nerve agents. *Acc. Chem. Res.* **45,** 756–766 (2012).

9. Gupta, R. D. *et al.* Directed evolution of hydrolases for prevention of G-type nerve agent intoxication. *Nat. Chem. Biol.* **7,** 120–5 (2011).

10. Yu, S. J. *The Toxicology and Biochemistry of Insecticides, Second Edition*. **24,** (CRC Press, 2014).

11. Wilkinson. *Insecticide Biochemistry and Physiology*. **11,** (Springer Science & Business Media, 2013).

12. Dickson, E. W. Diazepam Inhibits Organophosphate-induced Central Respiratory Depression. *Acad. Emerg. Med.* **10,** 1303–1306 (2003).

13. Cherny, I. *et al.* Engineering V-type nerve agents detoxifying enzymes using computationally focused libraries. *ACS Chem. Biol.* **8,** 2394–403 (2013).

14. Tsai, P.-C. *et al.* Stereoselective hydrolysis of organophosphate nerve agents by the bacterial phosphotriesterase. *Biochemistry* **49,** 7978–87 (2010).

15. Ghanem, E., Li, Y., Xu, C. & Raushel, F. M. Characterization of a phosphodiesterase capable of hydrolyzing EA 2192, the most toxic degradation product of the nerve agent VX. *Biochemistry* **46,** 9032–40 (2007).

16. Mee-Hie Cho, C., Mulchandani, A. & Chen, W. Functional analysis of organophosphorus hydrolase variants with high degradation activity towards organophosphate pesticides. *Protein Eng. Des. Sel.* **19,** 99–105 (2006).

17. Singh, B. K. & Walker, A. Microbial degradation of organophosphorus compounds. *FEMS Microbiol. Rev.* **30,** 428–71 (2006).

18. Pedroso, M. M. *et al.* Comparative investigation of the reaction mechanisms of the organophosphate-degrading phosphotriesterases from Agrobacterium radiobacter (OpdA) and Pseudomonas diminuta (OPH). *J. Biol. Inorg. Chem.* **19,** 1263–75 (2014).

19. Roodveldt, C. & Tawfik, D. S. Directed evolution of phosphotriesterase from Pseudomonas diminuta for heterologous expression in Escherichia coli results in stabilization of the metal-free state. *Protein Eng. Des. Sel.* **18,** 51–8 (2005).

20. Getzoff, E. D. *et al.* Electrostatic recognition between superoxide and copper, zinc superoxide dismutase. *Nature* **306,** 287–290 (1983).

21. Elcock, a H., Potter, M. J., Matthews, D. a, Knighton, D. R. & McCammon, J. a. Electrostatic channeling in the bifunctional enzyme dihydrofolate reductase-thymidylate synthase. *J. Mol. Biol.* **262,** 370–374 (1996).

22. Zeke, A., Lukács, M., Lim, W. A. & Reményi, A. Scaffolds: interaction platforms for cellular signalling circuits. *Trends Cell Biol.* **19,** 364–74 (2009).

23. Funabashi, H., Yanagi, S., Suzuki, S., Mie, M. & Kobatake, E. Assembly of zinc finger motif-fused enzymes on a dsDNA scaffold for catalyzing consecutive reactions with a proximity effect. *Biotechnol. Lett.* **37,** 109–14 (2015).

24. Genzer, J. & Bhat, R. R. Surface-bound soft matter gradients. *Langmuir* **24,** 2294–317 (2008).

25. Yonet-Tanyeri, N., Evans, R. C., Tu, H. & Braun, P. V. Molecular transport directed via patterned functionalized surfaces. *Adv. Mater.* **23,** 1739–43 (2011).

26. Wing, R. *et al.* Crystal structure analysis of a complete turn of B-DNA. *Nature* **287,** 755–758 (1980).

27. Reddy, B. S. P., Sharma, S. K. & Lown, J. W. Recent Developments In Sequence Selective Minor Groove DNA Effectors. *Curr. Med. Chem.* **8,** 475–508 (2000).

28. Gao, Y. *et al.* Tuning Enzyme Kinetics through Designed Intermolecular Interactions Far from the Active Site. *ACS Catal.* **5,** 2149–2153 (2015).

29. Morris, G. M. *et al. AutoDock 4.2 User Guide*. (2014). at <http://autodock.scripps.edu/faqs-help/manual/autodock-4-2-user-guide>

30. Wienken, C. J., Baaske, P., Rothbauer, U., Braun, D. & Duhr, S. Protein-binding assays in biological liquids using microscale thermophoresis. *Nat. Commun.* **1,** 100 (2010).

31. Shen, H. Y., Shao, X. L., Xu, H., Li, J. & Pan, S. D. In vitro study of DNA interaction with trichlorobenzenes by spectroscopic and voltammetric techniques. *International Journal of Electrochemical Science* **6,** 532–547 (2011).

32. Hajian, R., Shams, N. & Parvin, A. DNA-binding Studies of Daunorubicin in the Presence of Methylene Blue by Spectroscopy and Voltammetry Techniques. *Chinese J. Chem.* **27,** 1055–1060 (2009).

33. Kypr, J., Kejnovská, I., Renciuk, D. & Vorlícková, M. Circular dichroism and conformational polymorphism of DNA. *Nucleic Acids Res.* **37,** 1713–25 (2009).

34. Sabolová, D. Spectroscopic Studies of the Bis-3,6-Alkylamidoacridines as Potential Topoisomerase I Inhibitors. *Biochem. Physiol. Open Access* **02,** (2013).

35. Dijk, M. van & Bonvin, A. M. J. J. 3D-DART: a DNA structure modelling server. *Nucl. Acids Res.* W235–W239 (2009). doi:10.10193/nar/gkp287

36. Gaffarogullari, E. C., Krause, A., Balbo, J., Herten, D.-P. & Jäschke, A. Microscale thermophoresis provides insights into mechanism and thermodynamics of ribozyme catalysis. *RNA Biol.* **10,** 1815–21 (2013).

37. Shahabadi, N. & Hadidi, S. Spectroscopic studies on the interaction of calf thymus DNA with the drug levetiracetam. *Spectrochim. Acta. A. Mol. Biomol. Spectrosc.* **96,** 278–83 (2012).

38. Marty, R. *et al.* Structural analysis of DNA complexation with cationic lipids. *Nucleic Acids Res.* **37,** 849–57 (2009).

39. Agarwal, S., Jangir, D. K., Mehrotra, R., Lohani, N. & Rajeswari, M. R. A Structural Insight into Major Groove Directed Binding of Nitrosourea Derivative Nimustine with DNA: A Spectroscopic Study. *PLoS One* **9,** e104115 (2014).

40. Mati, S. S., Roy, S. S., Chall, S., Bhattacharya, S. & Bhattacharya, S. C. Unveiling the groove binding mechanism of a biocompatible

naphthalimide-based organoselenocyanate with calf thymus DNA: an ‘ex vivo’ fluorescence imaging application appended by biophysical experiments and molecular docking simulations. *J. Phys. Chem. B* **117,** 14655–65 (2013).

41. Wu, D. & Chen, Z. Study on the interaction between ginsenoside Rh2 and calf thymus DNA by spectroscopic techniques. *Luminescence* (2015). doi:10.1002/bio.2883

42. Li, H. *et al.* Interaction study of ciprofloxacin with human telomeric DNA by spectroscopy and molecular docking. *Spectrochim. Acta Part A Mol. Biomol. Spectrosc.* **107,** 227–234 (2013).

43. Zhang, Y., Zhang, G., Li, Y. & Hu, Y. Probing the binding of insecticide permethrin to calf thymus DNA by spectroscopic techniques merging with chemometrics method. *J. Agric. Food Chem.* **61,** 2638–47 (2013).

44. Veeralakshmi, S. *et al.* Single and double chain surfactant–cobalt(iii) complexes: the impact of hydrophobicity on the interaction with calf thymus DNA, and their biological activities. *RSC Adv.* **5,** 31746–31758 (2015).

45. Zhang, G., Fu, P. & Pan, J. Multispectroscopic studies of paeoniflorin binding to calf thymus DNA in vitro. *J. Lumin.* **134,** 303–309 (2013).

46. Das, T. *et al.* Phenazine virulence factor binding to extracellular DNA is important for Pseudomonas aeruginosa biofilm formation. *Sci. Rep.* **5,** 8398 (2015).

47. Dorraji, P. S. & Jalali, F. Investigation of the Interaction of Sertraline with Calf Thymus DNA by Spectroscopic Methods. *J. Braz. Chem. Soc.* **24,** 939–945 (2013).

APPENDICES

APPENDIX A: SUPPLEMENTAL FIGURES

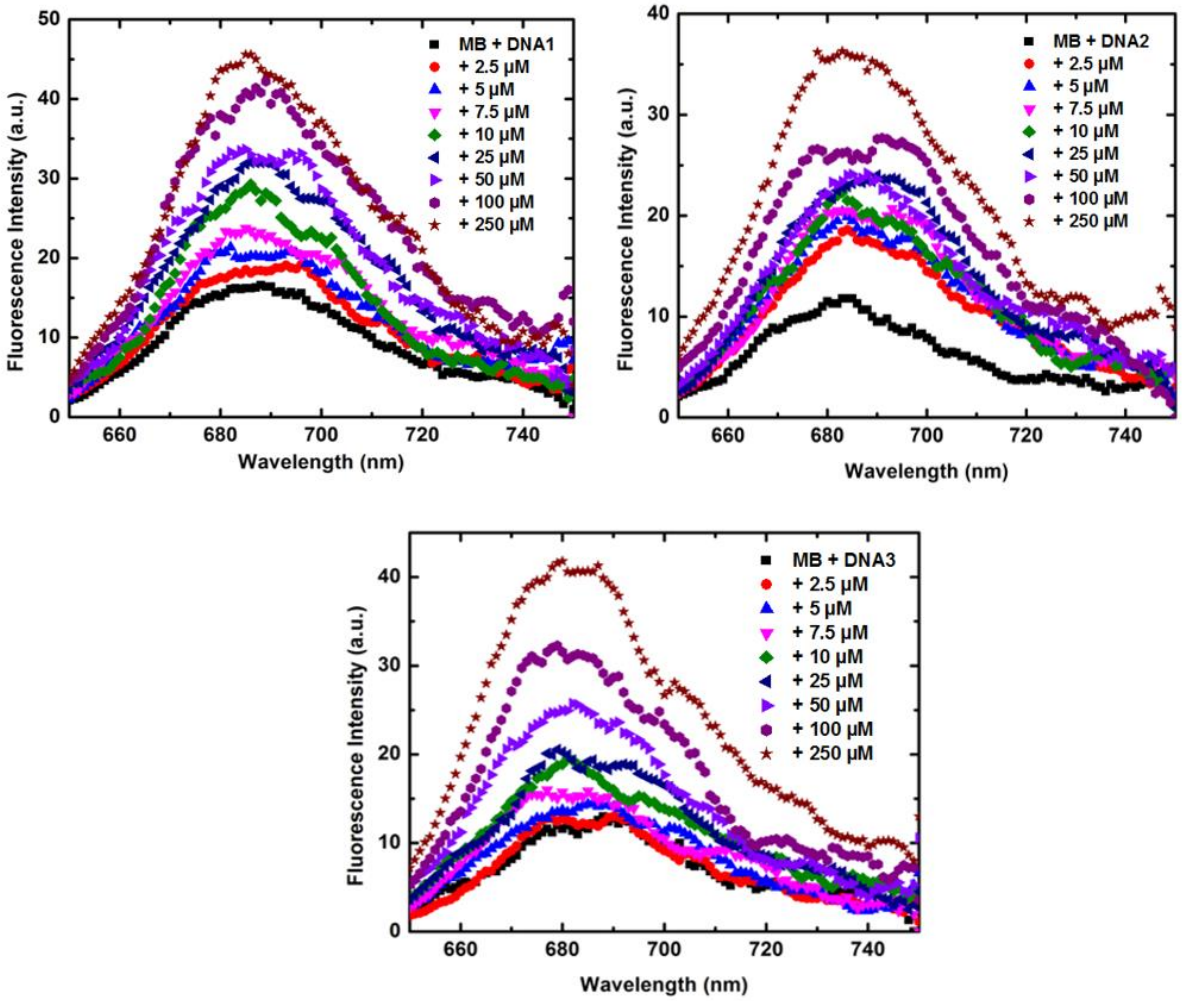

Figure A-1: Fluorescence emission with a constant concentration of methylene blue and DNA1 (top left), DNA2 (top right), and DNA3 (bottom center) with increasing paraoxon concentration (2.5, 5, 7.5, 10, 25, 50, 250 µM).

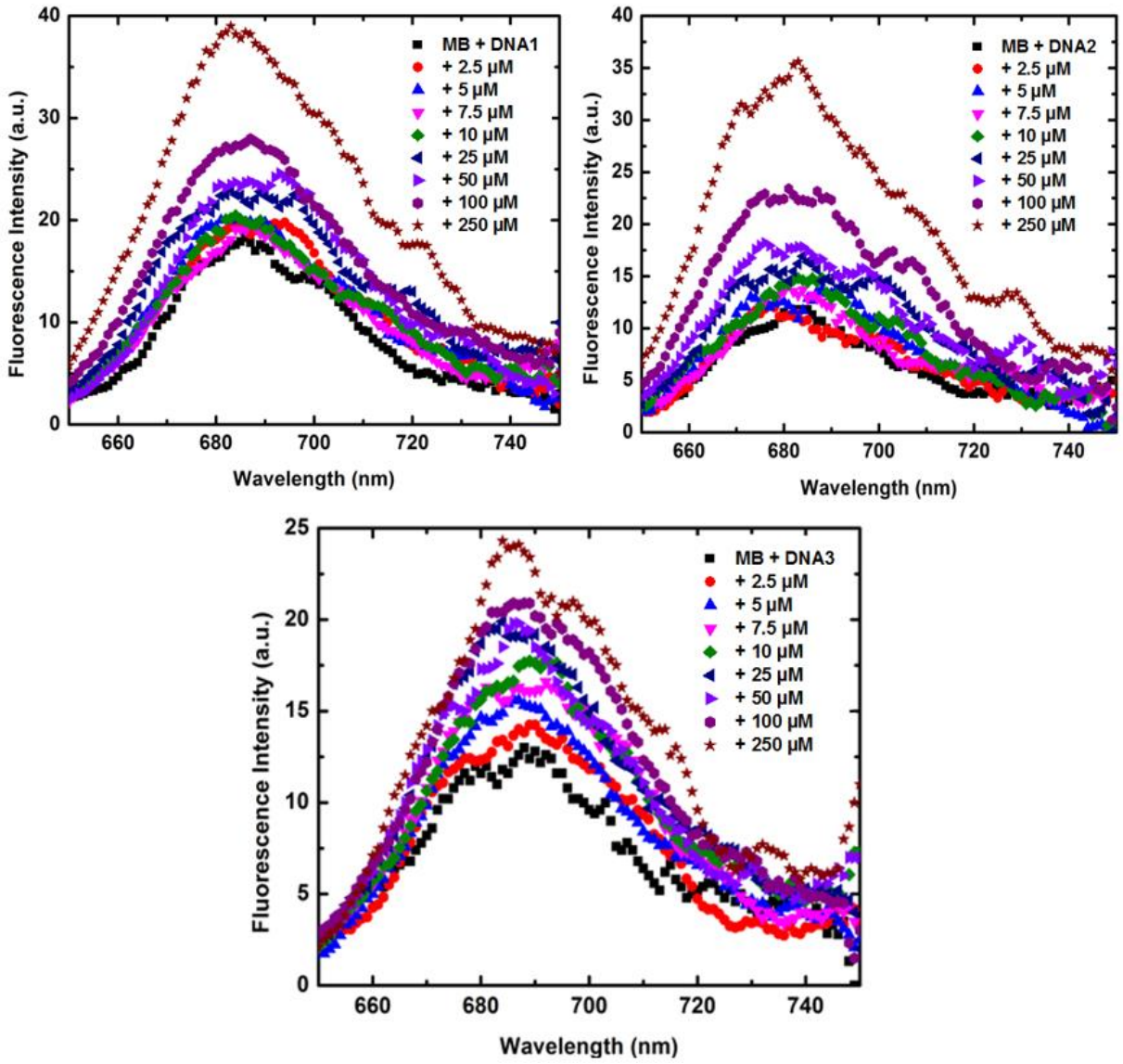

Figure A-2: Fluorescence emission with a constant concentration of methylene blue and DNA1 (top left), DNA2 (top right), and DNA3 (bottom center) with increasing p-nitrophenol concentration (2.5, 5, 7.5, 10, 25, 50, 250 µM).

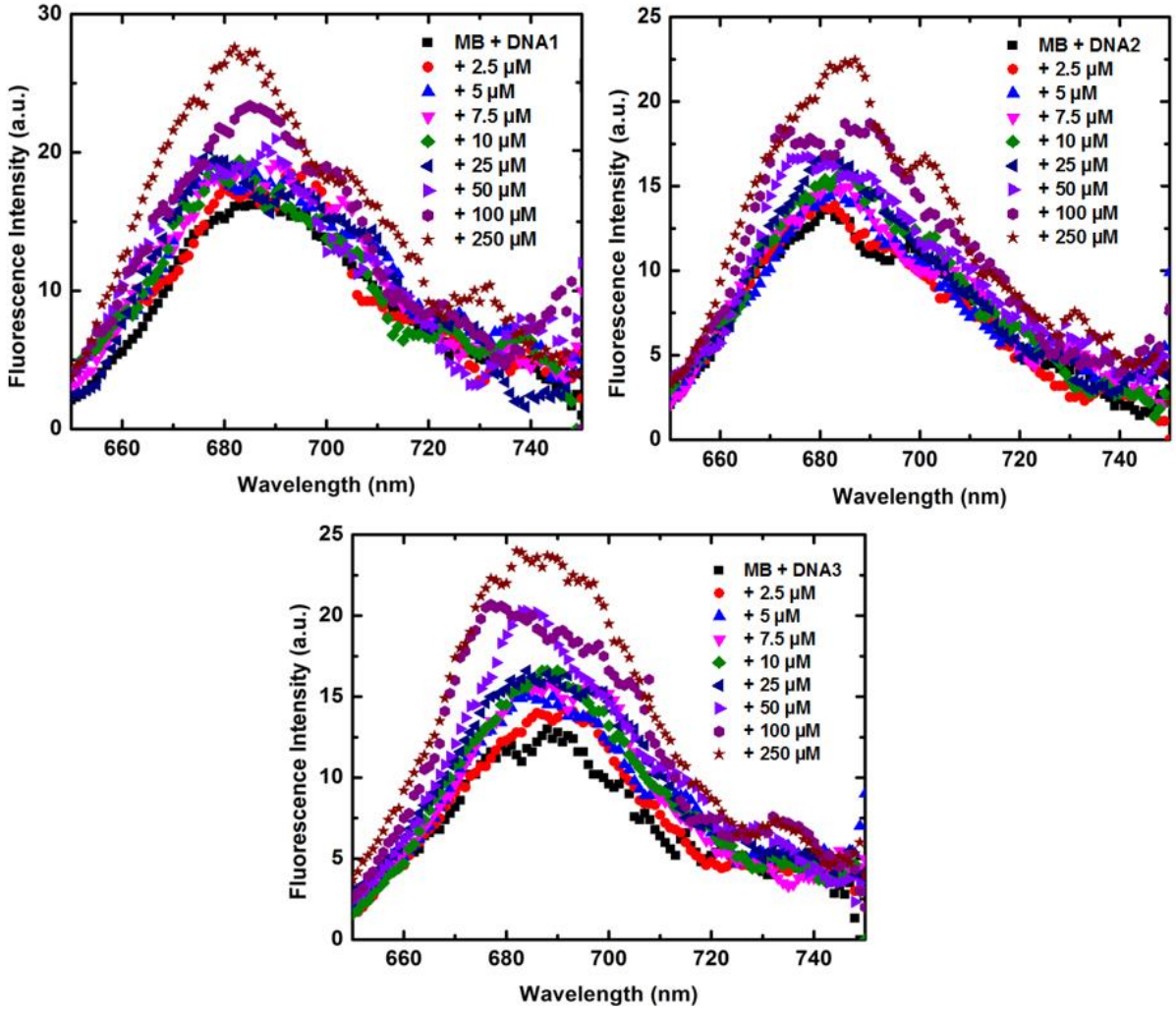

Figure A-3: Fluorescence emission with a constant concentration of methylene blue and DNA1 (top left), DNA2 (top right), and DNA3 (bottom center) with increasing methyl parathion concentration (2.5, 5, 7.5, 10, 25, 50, 250 µM).

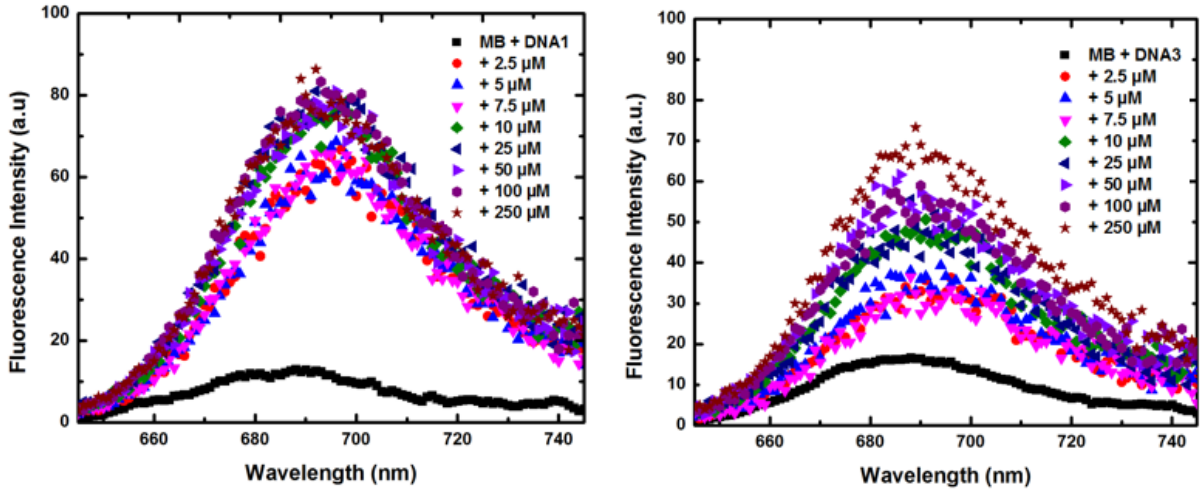

Figure A-4: Fluorescence emission with a constant concentration of methylene blue and DNA1 (left) and DNA3 (right) with increasing fensulfothion concentration (2.5, 5, 7.5, 10, 25, 50, 250 µM).